1   **Title:** Links between spatially heterogeneous pore water geochemistry, fluid migration, and
2   methane hydrate near a seafloor mound venting structure on the south Chilean Margin (41°S)

3   **Authors: Authors:** Vincent J. Clementi[1*], Yair Rosenthal[1,2], Samantha C. Bova[1,3], James D.
4   Wright[2], Elizabeth K. Thomas[4], Richard A. Mortlock[2], Owen C. Cowling[4], Linda V. Godfrey[2],
5   Laurel B. Childress[5], and Expedition 379T Scientists

6   **Affiliations**
7   [1]Department of Marine and Coastal Sciences, Rutgers University, New Brunswick, NJ
8   (*Corresponding author: clementi@marine.rutgers.edu)
9   [2]Department of Earth and Planetary Sciences, Rutgers University, Piscataway, NJ
10   [3]Present address: Department of Geological Sciences, San Diego State University, San Diego, CA
11   [4]Department of Geology, University at Buffalo, Buffalo, NY
12   [5]International Ocean Discovery Program, Texas A&M University, College Station, TX

13   **Key Points:**
14   **1)** Sediment cores taken <10 km apart near a seafloor mound venting structure have different pore
15   water chemistry
16   **2)** Pore water freshening is attributable to clay dehydration at depth, manifesting in fluid discharge
17   at the venting structure
18   **3)** Active fluid and gas migration may support the formation of methane hydrate near the mound

19   **Abstract**
20   Pore water freshening (i.e., decreases in dissolved Cl^-) has been documented in marine sediments
21   along most active margins, with the migration of deep fluids or methane hydrate dissociation often
22   invoked as sources of freshening in the sediment column. During D/V *JOIDES Resolution*
23   Expedition 379T in 2019, two new sites (J1005 and J1006) were cored near ODP Site 1233 (41°S),
24   adjacent to a seafloor mound venting structure. The three sites are less than 10 km apart but show
25   marked differences in pore water chemistry and methane hydrate occurrence. The extent of Cl^-
26   decrease is a function of distance from the mound, with the strongest freshening occurring at the
27   closest site (J1006), which is the only site where methane hydrate was observed. Methane fluxes
28   follow the same pattern, suggesting a common control. Increasing oxygen and decreasing
29   hydrogen isotopes point to deep mineral bound water as the primary source of freshening near the
30   mound, with fluids originating ~2.5 km below seafloor near the décollement. Secondary
31   contributions from methane hydrate dissociation and ash diagenesis also appear to influence
32   regional pore water chemistry. The variability in pore water freshening suggests that fluid
33   migration and eventual expulsion at the venting structure follows narrow pathways, likely along
34   faults within the forearc complex. The migration of deep, gas-charged fluids may also support
35   methane hydrate saturations greater than *in situ* organic carbon diagenesis would allow, but
36   nonetheless consistent with geophysical estimates. Together, the data highlight an important link
37   between fluid migration and methane hydrate formation on the Chilean Margin.
38

39   **Plain Language Summary**
40   The Chilean Margin is one of the world's largest subduction zones and has a substantial methane
41   hydrate reservoir at shallow depths in the sediment column. However, it is still poorly understood
42   how methane hydrate forms here since organic carbon content is low. We use the chemical

43   composition of marine sedimentary pore water to show that fresh, gas-rich fluid migrates from
44   much deeper in the sediment column to shallow depths where methane hydrate has been observed.
45   Our results suggest that this might be one such way that methane hydrate forms in higher
46   saturations than anticipated.

1. Introduction

Compressional tectonics, sediment loading, and the subsequent reductions in porosity are the principal processes controlling the vertical migration of fluids and gas through accreted sediments at convergent margins [*Moore and Vrolijk*, 1992]. Within these forearc complexes, the circulation and alteration of fluids can influence subduction mechanics and the cycling of elements between the ocean, lithosphere, and mantle [*Chan and Kastner*, 2000; *Peacock*, 1990; *Saffer and Tobin*, 2011]. At the sediment-seawater interface, fluids and gas can be expelled to the ocean through various seafloor venting structures like cold seeps and submarine mud volcanoes, which have been documented globally [*Brown*, 1990; *Kopf*, 2002; *Milkov*, 2000]. Provided sufficient volumetric fluxes, the transfer of fluid from sedimentary to oceanic regimes through these structures could exert influence on marine elemental and isotopic budgets [*Elderfield et al.*, 1990; *Gieskes et al.*, 1989; *Kastner et al.*, 1991].

Prior examination of pore water chemistry near seafloor venting structures have offered a better understanding of the hydrogeological and geochemical processes taking place well beyond the limits of modern ocean drilling [*Dahlmann and de Lange*, 2003]. The elemental and isotopic composition of these fluids often reflect subduction mechanics, diagenetic reactions, and mineral dehydration processes taking place deep within the accretionary prism. Indeed, pore water studies on the Barbados, Mediterranean, Nankai, Gulf of Cadiz, and Taiwan accretionary prisms (among others) have provided critical insight on the roles of dewatering in megathrust tectonism, fluid expulsion in oceanic geochemical budgets, and deep gas migration in supporting methane hydrate formation [*Chen et al.*, 2020; *Deyhle and Kopf*, 2001; *Dia et al.*, 1999; *Godon et al.*, 2004; *Haese et al.*, 2006; *Hensen et al.*, 2007; *Kopf and Deyhle*, 2002; *Martin et al.*, 1996; *Menapace et al.*, 2017; *Nishio et al.*, 2015; *Scholz et al.*, 2009; *Vanneste et al.*, 2011].

Despite these advances, the south Chilean Margin—a 1500 km convergent plate boundary and one of the most tectonically-active regions on Earth [*Melnick et al.*, 2006; *Völker et al.*, 2013]— remains one such setting where cold seeps and mud volcanoes have only been documented within a limited sector of the margin near the Concepción Methane Seep Area (36°S) [*Sellanes et al.*, 2004; *Vargas-Cordero et al.*, 2020]. Recently, cold seeps have also been observed near the Chile Triple Junction in the south (46°S) [*Villar-Muñoz et al.*, 2021]. The scarcity of documented venting systems is in stark contrast with fluid budget estimates in the forearc complex, which remain unbalanced and require transfer of fluid and volatiles from subducted sediments back to the ocean [*Volker et al.*, 2014]. Moreover, pore water studies near sites of active fluid and gas discharge on the Chilean Margin are limited [*Coffin et al.*, 2007; *Scholz et al.*, 2013; *Zheng et al.*, 1995]; thus, a comprehensive geochemical characterization of deep fluids remains incomplete. Addressing this deficiency can provide critical insight on a number of fronts, including the interaction between deep-seated fluids and tectonism on the Chilean Margin [*Contreras-Reyes et al.*, 2013; *Saffer and Tobin*, 2011; *Völker and Stipp*, 2015] and how fluid and gas migration within this accretionary prism supports a robust methane hydrate reservoir in shallow margin sediments despite relatively

85 low organic carbon content [*Brown et al.*, 1996; *Vargas-Cordero et al.*, 2017; *Vargas-Cordero et*
86 *al.*, 2021; *Villar-Muñoz et al.*, 2019].

87 Recent implementation of D/V *JOIDES Resolution* Expedition 379T (JR100) in July-August 2019
88 recovered 120 m sediment cores at Sites J1005 and J1006 (41°S) near the previously cored ODP
89 Site 1233 [*Bova et al.*, 2019]. The three sites are less than 10 km apart and underway seismic data
90 from this expedition, as well as ODP Leg 202 [*Mix et al.*, 2003], reveal that J1005, J1006, and
91 ODP 1233 are proximal to a ~4 km wide, ~25 m tall seafloor mound (Figure 1). The anticlinal
92 geometry of this sediment structure and observance of a gas flare just off axis of the meridional
93 seismic line suggest that this mound could be a mud volcano with active fluid and gas expulsion
94 occurring near the sites (Figure 1). However, the lack of documented mud breccia at any of the
95 three sites is in contrast with this interpretation, suggesting it could be a cold seep instead. In the
96 absence of higher resolution seismic data to better characterize this structure, we broadly define
97 the observed mound as a "seafloor venting structure".

98   Despite the proximity of these three sites to both the mound structure and each other (Table 1),
99   Sites J1005, J1006, and ODP 1233 have distinct pore water chemical compositions, most notably
100 in the downcore chloride concentration (Figure 1), which may indicate spatial heterogeneities in
101 fluid migration within this sector of the forearc complex. In this paper, we report on high-resolution
102 pore water elemental and isotope data from Sites J1005 and J1006, with the objectives to: (1)
103 characterize the source(s) of pore fluids in the vicinity of this mound using the elemental and
104 isotopic (oxygen, hydrogen, and strontium) composition of pore waters; (2) constrain fluid
105 migration pathways and reasons for spatially variable pore water chemistry; and (3) assess how
106 fluid and gas transport near venting structures on the Chilean Margin might support regional
107 methane hydrate formation.

108 **2. Study Area**
109 *2.1 Geologic and tectonic setting*
110 The south Chilean Margin (32–46°S) is one of the longest convergent continental margins on
111 Earth. Here, subduction of the Nazca plate beneath the South American plate is rapid (66 mm yr^{-}
112 ^{1}) and the region has produced some of the most destructive earthquakes in recent history (e.g.,
113 M_W 9.5, Valdivia, 1960; M_W 8.8, Maule, 2010) [*Melnick et al.*, 2006; *Völker et al.*, 2013].
114 Hemipelagic sedimentation along the Chilean Margin reflects influences from the regional
115 hydroclimate and steep catchment basins along the coastline. Prevailing westerlies yield annual
116 rainfall in excess of 7,500-10,000 mm yr^{-1} [*Garreaud et al.*, 2013], resulting in extensive erosion
117 and deposition of 21 km^3 yr^{-1} terrigenous material rich in detrital clays (e.g., smectite) [*Lamy et*
118 *al.*, 1998]. Frontal accretion and high sedimentation rates have manifested in the complete burial
119 of the structural trench and the development of a prominent forearc complex perpendicular to the
120 trench [*Maksymowicz*, 2015; *Völker et al.*, 2013]. This consists of an active accretionary prism that
121 is ~25 km wide and 2.5-3 km thick; the broader forearc complex is ~60 km wide and ~20 km thick

122 at its thickest, extending from the upper continental slope and shelf to the décollement [*Geersen*
123 *et al.*, 2011; *Völker et al.*, 2011].

124 Active subduction and frequent megathrust earthquakes have manifested in normal and splay
125 faulting throughout the forearc complex [*Völker et al.*, 2014]. Gas seepage on the south Chilean
126 Margin was first reported by Sellanes et al. [2004] in what is now called the Concepción Methane
127 Seepage Area (CMSA), with more recent evidence for active and paleo seepage [*Klaucke et al.*,
128 2012]. Seepage of methane-rich fluids typically cluster near these faults and support robust
129 chemosynthetic communities near the seafloor [*Munoz et al.*, 2016; *Sellanes et al.*, 2008]. It has
130 been suggested that onset of seepage in this region may be linked to the tectonic history of the
131 margin, potentially as recent as the 2010 Maule earthquake in some sectors of the margin [*Geersen*
132 *et al.*, 2016; *Villar-Muñoz et al.*, 2021]. Low pore water chloride concentrations in a small set of
133 multicores near the CMSA were interpreted to reflect freshening from deep fluids released during
134 clay dehydration processes at depth, potentially providing a mechanism for vertical migration of
135 gas saturated fluids at these seeps [*Scholz et al.*, 2013]. However, pore water freshening is not a
136 necessarily widespread feature at venting sites [*Coffin et al.*, 2007]. In contrast, high $^{18}O/^{16}O$ and
137 $^{2}H/^{1}H$ ratios ($\delta^{18}O$ and δD, respectively) in pore waters near a newly discovered chain of small
138 (meter-scale) mud volcanoes upslope and just south of the CMSA indicate that regional fluid
139 migration and discharge may be linked to methane hydrate dissociation [*Vargas-Cordero et al.*,
140 2020].

141 Methane hydrates are ubiquitous on the south Chilean Margin and have often, but not only, been
142 observed near sites of active venting [*Bangs et al.*, 1993; *Behrmann et al.*, 1992; *Coffin et al.*,
143 2007; *Vargas-Cordero et al.*, 2010; *Vargas-Cordero et al.*, 2017; *Villar-Muñoz et al.*, 2018; *Villar-*
144 *Muñoz et al.*, 2019]. Steep redox gradients indicate that marine sediments in the region are highly
145 reducing owing to sediment loading and microbial degradation of organic carbon (~0.5-2 wt%)
146 [*Bova et al.*, 2019; *Mix et al.*, 2003; *Scholz et al.*, 2013]. Anaerobic oxidation of methane (AOM)
147 from sulfate reduction typically occurs in the upper few meters of the sediment column, with
148 methanogenic conditions below [*Bova et al.*, 2019; *Coffin et al.*, 2007; *Mix et al.*, 2003; *Scholz et*
149 *al.*, 2013]. A widespread bottom simulating reflector marks the transition between methane
150 hydrate-rich sediments and free gas below [*Rodrigo et al.*, 2009]. On the Chilean Margin, this
151 horizon is relatively shallow, typically less than 150 meters below sea floor (mbsf), with methane
152 hydrate occupying 5-15% of the pore space [*Alessandrini et al.*, 2019; *Vargas-Cordero et al.*,
153 2017]. Sites of active venting often have the shallowest sulfate-methane transition zone, which can
154 be <1 mbsf or even at the sediment-seawater interface itself owing to high vertical fluxes of gas-
155 saturated fluids [*Coffin et al.*, 2007]. Elevated pore water alkalinity concentrations have been
156 observed throughout much of the margin, which likely reflect AOM via sulfate reduction but could
157 also be attributed to marine silicate weathering in the anoxic sedimentary system [*Torres et al.*,
158 2020; *Wallmann et al.*, 2008]. The alkalinity generated by these processes promote authigenic
159 carbonate precipitation below the SMTZ or even on the seafloor [*Bohrmann et al.*, 1998; *Klaucke*

160 *et al.*, 2012]. Similarly, methane hydrate near the CMSA can be found at or within a few meters
161 of the seafloor [*Vargas-Cordero et al.*, 2020].

162 ### *2.2 Study sites*
163 D/V *JOIDES Resolution* Expedition 379T (JR100) cored two sites at 41°S on the Chilean Margin.
164 Sites J1005 and J1006 are located on a bench in the upper continental slope ~38 km offshore at
165 807- and 824-meters water depth, respectively (Figure 1; Table 1). Three holes (A, B, and C) were
166 cored at each site using the advanced piston coring system, yielding complete stratigraphic sections
167 of 118 mbsf at J1005 and 120 mbsf at J1006. Sediment at both sites are assigned to single lithologic
168 units comprising of Pleistocene silty clay, with varying contributions from biogenic, volcanogenic,
169 and authigenic (sulfidic, silicate, carbonate) components. Despite the proximity of the sites, the
170 respective sediment columns have different bottom ages as indicated by shipboard correlation of
171 paleomagnetic and physical properties data [*Bova et al.*, 2019] (Table 1).

172 Site J1006 is located near the apex of a seafloor mound, with Site J1005 positioned just upslope
173 from this feature. Authigenic carbonate nodules were recovered at both sites (Figure S1); at J1005,
174 small (1-3 cm) concretions were recovered ~30-60 mbsf, with larger concretions (5-13 cm) and an
175 order of magnitude greater abundance at Site J1006 between 75-115 mbsf. Shipboard x-ray
176 diffraction (XRD) analysis indicates that these authigenic carbonates are primarily dolomitic in
177 composition [*Bova et al.*, 2019]. Likewise, methane hydrate nodules were recovered at Site J1006
178 ~85 mbsf (Figure S1). Sediment in the core sections within ±10 m of the hydrate interval was
179 heavily cracked and expanded owing to depressurization of gas (and potentially methane hydrate
180 dissociation) upon recovery (Figure S1). As a result, a substantial void between 88-104 mbsf exists
181 at J1006. Intact bivalve fossils were recovered at Sites J1005 and J1006 and were identified to
182 belong to the *Lucinidae* family of seawater clams (Figure S1). These burrowing bivalves live in
183 reducing, sulfur-rich sediments and can be indicative of active (or past) seepage of gas-saturated
184 fluids from the seafloor [*Holmes et al.*, 2005]. Full site reports are provided in the Expedition 379T
185 Preliminary Report [*Bova et al.*, 2019].

186 Sites J1005 and J1006 were cored 10 km and 5 km SSE of ODP Site 1233, respectively, which
187 was previously cored during ODP Leg 202 [*Mix et al.*, 2003]. Collectively, the three sites comprise
188 a lateral transect across the mound structure, with J1006 the most proximal, followed by ODP Site
189 1233 (<5 km), and J1005 being the most distal (~10 km) (Table 1). Like the JR100 sites, a shallow
190 SMTZ, methanogenic sediments, and authigenic carbonates were reported at ODP Site 1233 but
191 methane hydrate was not recovered despite strong reductions in pore water chloride concentration
192 >60 mbsf [*Mix et al.*, 2003]. The proximity of the three sites to the mound, similar lithologic and
193 depositional features, and similar redox conditions but distinct pore water chemistry makes these
194 sites uniquely suited to address the targeted research objectives outlined above.

195 ### 3. Materials and Methods

196   *3.1 Pore water sample collection for Sites J1005 and J1006*
197   Whole round samples (5-10 cm) were immediately collected from the bottom of each 1.5 m core
198   section upon recovery to the catwalk. A mudline sample was collected from Holes A and B in
199   J1005 and J1006. Whole rounds were sealed and transferred to the shipboard geochemistry
200   laboratory for processing. In total, 65 samples were taken from J1005 and 66 from J1006, with 13
201   and 14 analyzed onboard for interstitial water chemistry, respectively. The remainder of the pore
202   water samples were split (~4-10 mL each), sealed in airtight glass vacuoles, and archived for shore-
203   based isotope analysis.

204   For samples that underwent shipboard analysis, the sediment surface was carefully scraped and
205   removed to prevent contamination. The sample was then placed in a titanium hydraulic press and
206   subjected to 35,000 lb force for pore water extraction. Extraction fluid was filtered through a
207   Whatman No. 1 filter (11 μm) and 0.5 mL was discarded to avoid contamination. The remaining
208   fluid was filtered into a sterile syringe and filtered again through a 0.45 μm polysulfone filter prior
209   to shipboard analyses (or sample archiving).

210   *3.2 Shipboard pore water ion analysis*
211   Shipboard ion analysis of pore waters followed protocols outlined in Gieskes et al. [1991], Murray
212   et al. [2000], and the International Ocean Discovery Program user manual for shipboard
213   instrumentation. Major cation (Na, Ca, Mg, K) and anion (Cl^- and SO_4^{2-}) concentrations were
214   measured using a shipboard Metrohm 850 professional ion chromatographer (IC). Dissolved
215   ammonium (NH_4^+) concentrations were determined using an Agilent Cary Series 100 UV-visible
216   spectrophotometer fitted with an Agilent SPS3 autosampler. Alkalinity was determined
217   immediately after squeezing by Gran titration with an autotitrator (Metrohm 794 basic Titrino)
218   using 0.1M HCl at 25°C. Certain trace element (Li, Sr, B, dissolved silica (DSi)) concentrations
219   were measured using a shipboard Agilent 5110 SVDV ICP-AES. Precision (1σ) based on repeated
220   measurements of IAPSO and internal standards were <3.5% for IC measurements, <3.4% for
221   NH_4^+, and <2% for alkalinity. Reproducibility for ICP-AES measurements was ~1% for all
222   elements. We refer the reader to the Expedition 379T Preliminary Report for additional details on
223   shipboard geochemical analysis of pore water and sediment samples [*Bova et al.*, 2019].

224   *3.3 Pore water oxygen and hydrogen isotope analysis*
225   Pore water $\delta^{18}O$ and δD composition was determined using a Picarro L2130-*i* cavity ringdown
226   laser spectrometer light isotope instrument in triplicate at the University at Buffalo following
227   methods in van Geldern and Barth [2012] (J1005, n=13; J1006, n=22). Samples were injected four
228   times; each injection was corrected for memory, drift, and were then normalized to Vienna
229   Standard Mean Ocean Water (VSMOW). The first injection was discarded for each sample and
230   the remaining three analyses were aggregated into an average value with associated replicate
231   uncertainty. Average replicate standard deviation (1 SD) was 0.03‰ for $\delta^{18}O$ measurements and
232   0.11‰ for δD measurements.

233 Additional pore water $\delta^{18}O$ measurements (J1005, n=24; J1006, n=39) were made at the Rutgers
234 University Stable Isotope Laboratory using a FISONS OPTIMA Mass Spectrometer equipped with
235 a MicroMass mulitprep automatic sample processing system after 1-minute water equilibration
236 with CO_2 in a sealed glove bag using standard methods [*Epstein and Mayeda*, 1953; *Fairbanks*,
237 1982]. All samples were run in duplicate. Reproducibility is estimated to be ±0.04‰ (1 SD) as
238 determined by multiple (n=12) daily analyses of laboratory standards. Accuracy is estimated to be
239 within 0.03‰ by comparison of North Atlantic Bottom Water with VSMOW.

240 Lastly, a ~5 cm methane hydrate nodule was recovered from Hole C at Site J1006 (Figure S1) and
241 subsequently processed, archived, and analyzed for its $\delta^{18}O$ (Picarro and IR-MS) and δD (Picarro
242 only) composition following the protocols outlined above.

243 *3.4 Pore water strontium isotope analysis*
244 Pore water strontium isotope ($^{87}Sr/^{86}Sr$) analysis followed the Sr separation protocol of Horwitz et
245 al. [1992] (J1005, n=12; J1006, n=12). Sample volumes were calculated from shipboard elemental
246 concentrations, targeting at least 1 µg Sr for each sample. Pore water samples were acidified to 2N
247 strength with calculated volumes of 7N HNO_3 prior to separation. Strontium was
248 chromatographically separated from the pore water matrix using Eichrom 50-100 µm Sr Resin and
249 different concentrations of HNO_3. Strontium was collected in 0.05N HNO_3 in acid cleaned 3 mL
250 Savillex vials, dried down, and then dissolved in 2% by volume HNO_3 for analysis. Samples were
251 analyzed in a wet plasma using a ThermoScientific Neptune Plus MC-ICP-MS at Rutgers
252 University. Sr isotopes were corrected for fractionation using the measured $^{88}Sr/^{86}Sr$ ratio of
253 8.3752. NIST SRM 987, which was analyzed multiple times during sample analyses, yielded an
254 $^{87}Sr/^{86}Sr$ ratio of 0.710274±0.000008 (2 SD, n=13).

255 *3.5 Headspace hydrocarbon gas analysis*
256 Sediment gas composition was determined at a resolution of 1 sample per core for J1005 (n=11)
257 and J1006 (n=11). A 3 cm^3 bulk sediment sample was collected from the freshly exposed top end
258 of a core section using a brass boring tool immediately after core recovery on the catwalk. The
259 sediment plug was placed in a glass vial and sealed with an aluminum cap fitted with a
260 PTFE/silicon septa for transfer to the shipboard geochemistry laboratory. The vial was heated to
261 70°C for 30 minutes to evolve hydrocarbon gases from the sediment. A 5 cm^3 volume of headspace
262 gas was extracted from the sealed vial using a gas-tight 5 mL PTFE Luer lock glass syringe and
263 injected into the Agilent/HP 6890 Series II Gas Chromatograph fitted with a flame ionization
264 detector for analysis. Concentrations of methane (CH_4) and higher molecular weight hydrocarbons
265 (e.g., ethane, propane) were determined and reported as parts per million by volume (ppmv) of the
266 injected sample.

267 **4. Results and Discussion**

268   Pore water geochemical profiles for Sites J1005 and J1006 are shown in Figure 2 and Figure 3,
269   respectively [*Clementi et al.*, 2022b]. Despite the proximity of the two sites (<5 km), there exists
270   substantial spatial heterogeneity in pore water chemistry. Most notable is the difference in chloride
271   (Cl⁻) concentration, which at J1006 decreases from seawater values by ~200 mM with depth but
272   undergoes relatively little change at J1005. This ~37 percent decrease in Cl⁻ concentration suggests
273   mixing with a freshwater source. The freshening signal occurs concomitantly with marked changes
274   in the concentrations of Ca, Mg, K, B, DSi, Li, and Sr (Figure 3). Normalizing elemental
275   concentrations to Cl⁻ allows for comparison between the sites and reveals the conservative
276   behavior in pore fluid chemistry at J1005 compared with J1006 (Figure 2). Site J1005 is positioned
277   slightly upslope from J1006 and farther from the mound, and the pore water composition here
278   suggests minimal influence from deeper fluid sources in the cored strata. As such, we treat J1005
279   pore water as a reference site for pore waters near the mound venting structure, which provides
280   context for observed changes at J1006. In contrast, the non-conservative nature of pore waters at
281   J1006 suggests a complex sedimentary environment. Site J1006 is closest to the mound and the
282   strong freshening signal implies a dominant influence from venting-associated fluids on pore water
283   chemistry. However, downcore changes in elemental concentrations are not homogeneous (e.g.,
284   Mg/Cl and B/Cl) and potentially highlight multiple source fluids.

285   In the following sections, we use pore water $\delta^{18}O$ and δD to identify the source of low-Cl⁻ fluid at
286   Site J1006. Changes in the radiogenic strontium isotope ratio ($^{87}Sr/^{86}Sr$) can be independent from
287   changes in O/H isotopes and provide constraints on additional source fluids. Comparison with
288   elemental data from ODP Site 1233 offers context for spatial heterogeneity near the venting
289   structure. Finally, we use this information to address implications for fluid and gas migration in
290   the accretionary prism and how such processes might influence methane hydrate formation in the
291   region.

4.1 Source(s) of low Cl⁻ at J1006
293   Pore water freshening in convergent margin settings is often attributed to methane hydrate
294   dissociation and mineral dehydration (e.g., smectite to illite transformation, also referred to as
295   illitization), although clay membrane ion filtration, low-temperature crustal alteration, anaerobic
296   oxidation of methane, mixing with meteoric water have all been shown to yield Cl⁻ concentrations
297   lower than seawater in convergent margin sediments from Nankai Trough, the Cascadia and Peru
298   margins, Barbados, and the Mediterranean Sea [*Dahlmann and de Lange*, 2003; *Kastner et al.*,
299   1991; *Kastner et al.*, 1990; *Toki et al.*, 2017]. Indeed, prior pore water studies in this study region,
300   paired with lithologic evidence for abundant smectite content and recovered hydrate nodules, have
301   prompted hypotheses that documented freshening signals are primarily attributable to clay
302   dehydration or methane hydrate dissociation [*Bova et al.*, 2019; *Mix et al.*, 2003; *Scholz et al.*,
303   2013]. However, a 200 mM reduction in Cl⁻ concentration (similar in magnitude to Site J1006) at
304   a site offshore Patagonia was recently attributable to the deep submarine infiltration of fossil
305   groundwaters [*Clementi et al.*, 2022a]. This new finding challenges the basis of the longstanding

306 hypotheses in this region and implies that low Cl⁻ concentrations in pore waters cannot alone be
307 used to diagnose influences from illitization or methane hydrate dissociation, regardless of
308 additional sedimentary evidence.

309 The alteration processes that can yield low-Cl⁻ pore fluids isotopically fractionate oxygen and
310 hydrogen in distinct ways, which can enrich or deplete pore water $\delta^{18}O$ and δD relative to seawater
311 (Table S1). For example, compaction and increasing temperature (60-150°C) during slab
312 subduction promotes the dehydration of hydrous minerals, such as the alteration of smectite to
313 illite clays [*Perry*, 1970]. Relative to seawater, this mineral-bound water is enriched in $\delta^{18}O$ and
314 depleted in δD and is released to the surrounding sediments during dehydration reactions [*Savin*
315 *and Epstein*, 1970], which increases $\delta^{18}O$ and decreases δD in the pore water [*Kastner et al.*, 1991].
316 In contrast, methane hydrate dissociation increases both $\delta^{18}O$ and δD owing to fractionation of the
317 heavier isotopes into the hydrate matrix [*Hesse and Harrison*, 1981; *Ussler and Paull*, 1995].
318 Methane hydrate dissociation typically occurs from hydrostatic pressure decreases during core
319 recovery, which can result in anomalous pore water $\delta^{18}O$ and δD increases (and Cl⁻ decreases)
320 from otherwise conservative profiles (e.g., [*Egeberg and Dickens*, 1999; *Matsumoto and*
321 *Borowski*, 2000; *Torres et al.*, 2004]). In certain instances, however, *in situ* dissociation can occur
322 and produces more gradual changes in the downcore profiles (e.g., [*Vargas-Cordero et al.*, 2020]).

323 Methane hydrate nodules were only recovered at J1006, where there was substantial cracking and
324 expansion of core material from gas expansion (Figure S1). As such, we initially hypothesized that
325 the linear decrease in Cl⁻ with depth was attributable to *in situ* methane hydrate dissociation [*Bova*
326 *et al.*, 2019]. Indeed, decreases in Cl⁻ concentrations below 60 mbsf at ODP Site 1233 were also
327 attributed to active hydrate dissociation [*Mix et al.*, 2003]. The downcore $\delta^{18}O$ increase (0.5‰) at
328 J1006 is consistent with mixing between seawater and dissociated fluid as evidenced by a $\delta^{18}O$
329 value of 3.02‰ in the recovered methane hydrate nodule; this hydrate endmember value is in
330 agreement with observations in both laboratory and natural settings [*Davidson et al.*, 1983;
331 *Kvenvolden and Kastner*, 1990; *Martin et al.*, 1996]. In contrast, δD decreases by ~2‰ from
332 seawater values (Figure 3). Notwithstanding a few anomalously enriched $\delta^{18}O$ and δD values ~85-
333 90 mbsf, which most likely reflect hydrate dissociation upon recovery (i.e., hydrate δD value of
334 19.7‰), the robust downcore δD decrease appears to rule out a primary influence from *in situ*
335 methane hydrate dissociation on pore water freshening in the region. This requires an alternate
336 fluid source for low Cl⁻ concentrations at J1006 and ODP Site 1233.

337 We assess the relationship between pore water freshening (i.e., decreasing Cl⁻ concentrations) and
338 $\delta^{18}O$ increases and δD decreases at J1006 by comparing observed downcore changes (Cl$_{obs}$,
339 $\delta^{18}O_{obs}$, and δD_{obs}) with seawater reference values (Cl$_{ref}$, $\delta^{18}O_{ref}$, and δD_{ref}) [*Tomaru et al.*, 2006].
340 Downcore Cl⁻ concentration is normalized to seawater, yielding a freshening factor,
341 f([Cl$_{obs}$]/[Cl$_{ref}$]); the changes in $\delta^{18}O$ and δD ($\Delta\delta^{18}O$ and $\Delta\delta D$, respectively) are derived as δ_{obs}-δ_{ref}

342   [*Hong et al.*, 2021]. At Site J1006, this approach demonstrates that the observed $\delta^{18}O$ increase
343   (higher $\Delta\delta^{18}O$) and δD decrease (lower $\Delta\delta D$) with depth occurs as a function of pore water
344   freshening, as denoted by lower *f* (Figure 4), which suggests that the fresh mound-associated pore
345   fluid is primarily sourced from clay dehydration reactions at depth (Table S1). The alteration of
346   smectite to illite often involves the consumption of K from surrounding pore waters and release of
347   Li, B, DSi with the mineral bound water [*Chao et al.*, 2011; *Hüpers and Kopf*, 2012]. At J1006,
348   the linear K/Cl increase between 0-50 mbsf is driven by the marked decrease in Cl^- concentrations,
349   whereas the greatest consumption of K occurs below ~50 mbsf and results in a cessation of the
350   K/Cl increase (Figure 3; Figure S2). The increase in Li above seawater concentrations tracks the
351   decrease in Cl^- concentration, which results in an overall increase in Li/Cl and implies a deep Li
352   source. Similarly, downcore DSi and B concentrations increase substantially above seawater
353   values. These elemental profiles substantiate the robust isotopic evidence for dehydration reactions
354   sourcing the low-Cl^- fluids at Site J1006, and now adds the Chilean Margin to the large body of
355   evidence linking illitization to venting structures along convergent margins (e.g., [*Chao et al.*,
356   2011; *Chen et al.*, 2020; *Dahlmann and de Lange*, 2003; *Martin et al.*, 1996]).

357   At J1006, fluid endmember estimates by linear extrapolation of $\delta^{18}O$ and δD to zero Cl^-
358   concentration yield values of approximately +1‰ and -11.5‰ (Figure S3). Although fluid isotopic
359   endmembers for illitization on the Chilean Margin have not yet been established, these estimates
360   are different than the clay dehydration endmember derived using pore waters from the
361   Mediterranean Sea ($\delta^{18}O$: +10‰, δD: -32‰) [*Dahlmann and de Lange*, 2003]. This discrepancy
362   suggests that there may be additional fluid sources acting to modify pore water chemistry near the
363   mound. The bottom 20-30 m at J1006 is characterized by marked shifts in elemental concentrations
364   (e.g., Ca, Sr, Na, and B) and less radiogenic $^{87}Sr/^{86}Sr$ (Figure 3). The high Sr/Cl and low $^{87}Sr/^{86}Sr$
365   at depth are characteristic of ash alteration, although apparent consumption of Sr (and Ca) with
366   little change in $^{87}Sr/^{86}Sr$ between 10-80 mbsf (also at J1005) highlights a likely influence from
367   authigenic carbonate precipitation [*Elderfield and Gieskes*, 1982] (Figure 5).

368   Volcanogenic material comprised less than 10 percent of bulk sediment composition in cores
369   recovered during this expedition [*Bova et al.*, 2019]. However, even minor ash diagenesis can
370   impart large changes in pore water Sr and its isotopes [*Hong et al.*, 2020], as well as $\delta^{18}O$ and δD
371   [*Egeberg et al.*, 1990; *Lawrence and Gieskes*, 1981]. In contrast to clay dehydration, the formation
372   of hydrous minerals during ash diagenesis should decrease $\delta^{18}O$ and increase δD in surround pore
373   water [*Kastner et al.*, 1991] (Table S1). We suggest that an overprinting of ash alteration on the
374   primary signal from clay dehydration explains the discrepancy between endmember $\delta^{18}O$ and δD
375   estimates at J1006 and expected endmember values from the Mediterranean Sea, as well as the
376   abrupt changes in certain elemental concentration at depths greater than 100 mbsf. Low pore water
377    $\delta^{18}O$ and $^{87}Sr/^{86}Sr$ were also reported at ODP Sites 859 and 860 offshore Patagonia (46°S) and
378   were attributed to ash diagenesis [*Zheng et al.*, 1995], which suggests that diagenetic alteration of

379 volcanogenic material may be a common process on the south Chilean Margin but does not appear
380 to be occurring uniformly throughout the sediment column.

381 The lack of a similar elemental and isotopic signals at Site J1005 highlights the spatial
382 heterogeneity in regional pore fluid composition and migration. Here, $\delta^{18}O$ and δD have a
383 prominent maxima at ~25 mbsf (Figure 2), which is attributable to the downward diffusion of
384 isotopically heavier seawater during the last glacial period [*Adkins et al.*, 2002]. This feature is
385 also present at Site J1006, but the relatively higher $\delta^{18}O$ and lower δD peaks suggest active
386 migration of deep fluids with a distinct isotopic signature has likely attenuated the glacial signal.
387 That this signal is even present at J1006 might indicate that fluid discharge at this MV initiated at
388 some point since the last glaciation. Alternatively, enriched pore water $\delta^{18}O$ and δD paired with
389 low Cl^- concentrations could indicate *in situ* dissociation of methane hydrate, which would be
390 consistent with observations offshore Patagonia and near mud volcanoes proximal to the CMSA
391 [*Clementi et al.*, 2022a; *Ussler and Paull*, 1995; *Vargas-Cordero et al.*, 2020]. It is worth noting
392 that $\delta^{18}O$ and δD abruptly increase and decrease, respectively, at the very base of J1005 (Figure
393 2). These values agree with those at J1006 and suggest that deeply sourced fluids from clay
394 dehydration may also be influencing sediments farther from the mound. However, Cl^- (and other
395 elemental) concentrations near seawater values at this same depth indicate minimal influence on
396 pore water freshening (Figure 2; Figure S2), or that the locus of freshening at J1005 is deeper than
397 the recovered sediment column. Taken together, the new pore water elemental, $\delta^{18}O$, δD, and
398 $^{87}Sr/^{86}Sr$ profiles highlight a complex diagenetic environment and for the first time characterize
399 deep fluids being expelled at a seafloor venting structure on the Chilean Margin.

4.2 Constraints on fluid migration
401 Although no pore water isotope data have been reported for ODP Site 1233, the decreasing Cl^-
402 concentrations below 60 mbsf are paired with decreasing K and Li concentrations above seawater
403 concentrations [*Mix et al.*, 2003] (Figure 6). These downcore changes are consistent with profiles
404 at Site J1006 (Figure 3), which is located less than 5 km to the south. From this, we infer that low
405 Cl^- concentrations at ODP Site 1233 also reflect deep freshening influences from clay dehydration.
406 Indeed, the depth at which pore water Cl^- starts decreasing at ODP Site 1233 coincides with depths
407 in the sediment column at which seafloor reflectors begin dipping upwards; these horizons
408 intersect the seafloor near Site J1006 and implies a link between seafloor geometry and fluid flow
409 (Figure 1). The diminishing freshening signal with increasing distance from the mound
410 (J1006>ODP 1233>J1005) suggests that the migration of mound-associated fluids may be focused,
411 potentially aided by faults and the anticlinal sediment structure.

412 The alteration of smectite to illite takes place at sedimentary temperatures between 60-150°C
413 [*Perry*, 1970]. We apply the Na/K geothermometer to constrain temperatures at the depth of
414 illitization ($Z_{S \to I}$) [*Martin et al.*, 1996; *Nieva and Nieva*, 1987], which yield a consistent
415 equilibrium alteration temperature of 142±6°C amongst the three sites (Table 2). We refrained

416 from using Mg- or Ca-based geothermometers owing to the precipitation of authigenic carbonate
417 at Sites J1005 and J1006 [*Bova et al.*, 2019], which could bias the temperature estimate. The lack
418 of continuous Li enrichment with depth suggests that alteration temperatures are <150°C, in
419 agreement with our Na/K estimates [*Hensen et al.,* 2007]. Applying the Na/K-derived alteration
420 temperatures to geothermal gradients at the three sites demonstrates that $Z_{S \to I}$ is achieved 2.5±0.6
421 kmbsf, although different Na/K geothermometers provide a range of $Z_{S \to I}$ estimates between
422 2.4±0.6 and 2.7±0.7 kmbsf [*Fournier*, 1979; *Tonani*, 1980] (Table 2). Nonetheless, the $Z_{S \to I}$
423 estimates are more or less consistent with each other and thermal modeling estimates near the
424 CMSA ($Z_{S \to I}$ = 2-5 kmbsf) [*Scholz et al.*, 2013]. This places the locus of smectite dehydration
425 towards the base of the trench fill package near the décollement [*Völker et al.*, 2013], as observed
426 in the Barbados and Mediterranean accretionary complexes [*Martin et al.*, 1996; *Scholz et al.*,
427 2009].

428 Vertical fluid migration in accretionary prisms typically follows fault or fractures in the thrusted
429 sediment [*Moore and Vrolijk*, 1992]. We surmise that faults in this sector of the forearc complex
430 act as a conduit for deeply sourced fluids to vent at the seafloor. The mound near our sites appears
431 to be the seafloor manifestation of such migration and discharge. However, the observed variability
432 in downcore freshening at J1005, J1006, and ODP Site 1233 suggest that despite their proximity,
433 fluid migration pathways are potentially narrow.

434 *4.3 Implications for Chilean Margin methane hydrate formation*
435 Methane hydrate is ubiquitous on the south Chilean Margin, occupying ~7.5 percent of the pore
436 space on average but can range from 5-15 percent [*Alessandrini et al.*, 2019; *Villar-Muñoz et al.*,
437 2018; *Villar-Muñoz et al.*, 2019], with higher hydrate saturation (S_h) often reported near faults in
438 the forearc sediments [*Vargas-Cordero et al.*, 2018]. Methane hydrate typically forms in marine
439 sediments with relatively high total organic carbon (TOC) content (>2%) to supply sufficient
440 material for biogenic methane production [*Hesse and Harrison*, 1981; *Kvenvolden*, 1993]. In
441 contrast, TOC in sediments along the Chilean Margin is relatively low (0.2-2%, average of 0.87%
442 at the three sites) owing to high sedimentation rates and burial, with the highest TOC content
443 limited to the sediment-seawater interface [*Bova et al.*, 2019; *Mix et al.*, 2003; *Scholz et al.*, 2013]
444 (Figure S4). TOC can be used to provide a first-order approximation of S_h linked to *in situ* biogenic
445 methane production following:

446 $$S_h = 3.45 \cdot \text{TOC} - 1.77$$

447   [*Waseda*, 1998]. Average TOC content at the three sites would yield 1.2 percent of the pore space
448 occupied by methane hydrate, which is substantially lower than margin estimates (Figure S4).
449 Moreover, methane hydrate nodules were only recovered at Site J1006 but not at Site J1005 [*Bova*
450 *et al.*, 2019]; nor were they reported at ODP Site 1233 [*Mix et al.*, 2003]. This suggests that an
451 additional methane supply (independent from *in situ* biogenic generation) may be needed to

452 account for observed S_h estimates in the region, and that this additional source might also account
453 for spatially heterogeneous methane hydrate formation near the mound.

454 Deep fluids are often enriched in methane and the vertical migration of these fluids has been
455 suggested to facilitate the formation of methane hydrate near cold seep and mud volcano structures
456 globally [*Milkov*, 2000; *You et al.*, 2019]. On the Chilean Margin, AOM via sulfate reduction is
457 the dominant diagenetic pathway for deposited organic matter [*Treude et al.*, 2005], which leads
458 to rapid decreases in pore water sulfate concentration and increases in methane concentration,
459 resulting in shallow SMTZ depths as observed at our sites (Figure 6; Table 3). SMTZ depths follow
460 a similar pattern as downcore freshening, with the shallowest SMTZ at J1006, followed by ODP
461 Site 1233, and J1005 with the deepest (Table 3). Below the SMTZ, methane concentrations also
462 yield a similar trend, with the highest CH_4 concentrations at J1006 occurring as a sharp peak just
463 below the SMTZ, whereas broader and deeper maxima are observed at the more distal sites (Figure
464 6).

465 Assuming steady state conditions, the downward diffusion and consumption of pore water sulfate
466 is controlled by the upward diffusion of methane, allowing us to approximate the vertical methane
467 flux at each site [*Borowski et al.*, 1996]. Diffusive sulfate fluxes can be calculated following Fick's
468 first law:

469
$$J = -\emptyset \cdot D_s \cdot \frac{dC}{dz}$$

470 where J represents the downward sulfate flux (mmol m^{-2} yr^{-1}), $\emptyset$ is the average porosity between
471 the sediment-seawater interface and the SMTZ (dimensionless), D_s is the sediment diffusion
472 coefficient (cm^2 s^{-1}), and $\frac{dC}{dz}$ is the pore water sulfate concentration gradient between the sediment-
473 seawater interface and the SMTZ (mM cm^{-1}) [*Berner*, 1980]. D_s was corrected for tortuosity and
474 calculated assuming a tracer diffusion coefficient for sulfate following Boudreau [1997]:

475
$$D_s = \frac{D_0}{1 - \ln(\emptyset)^2}$$

476 where D_0, the diffusion coefficient for sulfate in seawater, is 5.8x10^{-6} cm^2 s^{-1} [*Li and Gregory*,
477 1974]. We assume a linear decrease in sulfate concentration between the sediment-seawater
478 interface and the SMTZ (Figure 6). Although sampling resolution in the upper few meters of
479 J1005, J1006, and ODP Site 1233 is relatively low, this assumption is substantiated by pore water
480 sulfate profiles from gravity cores taken near seep sites in the CMSA [*Coffin et al.*, 2007]. As such,
481 our calculated diffusion rates are taken as conservative flux estimates since complete sulfate
482 reduction near venting sites can occur even shallower than J1006 indicates, resulting in steeper
483 sulfate gradients in the upper few meters of the sediment column and higher flux estimates.

484   Downward sulfate diffusion rates range between -67.40 and -306.96 mmol m^{-2} yr^{-1}, with the
485   highest flux at J1006 and lowest at J1005 (Table 3). As expected, sulfate fluxes at ODP Site 1233
486   (-164.63 mmol m^{-2} yr^{-1}) fall between the other two sites. The sulfate flux at J1006 is consistent
487   with estimates from a seep site in the CMSA (-361.91 mmol m^{-2} yr^{-1}), which had a much shallower
488   SMTZ (33 cm) [*Coffin et al.*, 2007]. Assuming a 1:1 stoichiometric consumption of sulfate and
489   methane [*Borowski et al.*, 1996], and neglecting influences from advection that would likely
490   enhance the migration of deep fluids, we can infer that methane fluxes at J1006 are at least ~2 and
491   5 times greater than ODP Site 1233 and J1005, respectively. This provides a mechanism to
492   supplement the low methane concentrations/hydrate saturation solely from organic matter
493   degradation to concentrations that are likely sufficient to support the higher hydrate saturations
494   estimated in this region [*Alessandrini et al.*, 2019; *Vargas-Cordero et al.*, 2018; *Villar-Muñoz et*
495   *al.*, 2018; *Villar-Muñoz et al.*, 2019]. It is important to note that the lack of recovered methane
496   hydrate at J1005 and J1006 does not imply that they are not present. It is plausible, given the
497   widespread bottom simulating reflector along the Chilean Margin [*Rodrigo et al.*, 2009], that
498   methane hydrate could have simply been missed during coring operations at these sites or that they
499   could be limited to deeper sections of the sediment column than were cored. Nonetheless, pore
500   water elemental, isotopic, and hydrocarbon data from J1006 provide robust evidence that the
501   vertical migration of fresh, gas saturated fluids from deep within the forearc complex may be a
502   primary factor in the formation of shallower methane hydrate on the Chilean Margin (Figure 7).

503   The abundance of authigenic dolomitic concretions, as confirmed by shipboard XRD, at J1006
504   further supports active gas migration at this site. The absence of radiogenic pore water $^{87}Sr/^{86}Sr$
505   appears to rule out influences from anoxic marine silicate weathering as a control on alkalinity
506   production [*Torres et al.*, 2020; *Wallmann et al.*, 2008] (Figure 5). Instead, AOM via sulfate
507   reduction yields high pore water alkalinity concentrations at depth (Figure 6) following:

$$CH_4 + SO_4^{2-} \rightarrow HCO_3^- + HS^- + H_2O$$

509   [*Reeburgh*, 1980]. Marked downcore decreases in pore water Ca/Cl, Mg/Cl, and Sr/Cl ratios
510   (Figure 3) suggests that authigenic carbonate formation is also a sink for these divalent cations, in
511   particular between 50-100 mbsf where the highest density of concretions was documented [*Bova*
512   *et al.*, 2019]. Authigenic carbonates were also recovered at J1005 and ODP Site 1233 despite much
513   less (or no) pore water freshening (i.e., venting signals). Thus, migration pathways and/or
514   advective rates for gas saturated fluids at these sites may have been different in the past, with the
515   distribution of authigenic carbonates serving as potential paleo-horizons of shallow SMTZ depths
516   and venting [*Sample*, 1996]. Indeed, recovery of fossil *Lucinidae* shells and authigenic carbonate
517   nodules from ~55 mbsf at Site J1005 potentially indicate more active seepage in the past at this
518   site despite a lack of pore water freshening in the sediment column today [*Holmes et al.*, 2005]

519 (Figure S1). Geochemical characterization of authigenic carbonates and other minerals (e.g.,
520 sulfides) may provide valuable insight on the evolution of fluid venting on the Chilean Margin.

521 **5. Conclusions**
522 Pore waters from sediment cores at sites proximal to a mound venting structure on the south
523 Chilean Margin were collected and analyzed for their elemental and isotopic composition. The
524 downcore patterns of $\delta^{18}O$ and δD reveal the influence from deeply-rooted fluids linked to smectite
525 dehydration as a source of freshening in marine sediments. Strontium isotope systematics highlight
526 secondary influences from ash diagenesis on pore water chemistry. The extent of pore water
527 freshening and intensity of methane fluxes are a function of a site's distance to a regional seafloor
528 mound, with the largest decreases in Cl^- concentration and highest methane fluxes occurring
529 closest to this venting structure where methane hydrate was documented. This not only suggests
530 that subsurface fluid and gas migration within the accretionary prism may be directly linked to
531 venting structures, but also that delivery of fresh, gas-saturated fluids from deeper in the sediment
532 column may be a critical component of higher than estimate methane hydrate saturations on the
533 Chilean Margin. Together, the data paint a clearer picture of the mechanisms of fluid and gas
534 migration within the forearc complex.

546 [†]**Expedition 379T Scientists (those not listed above):** Ivano W. Aiello[1], Alejandro Avila[2],
547 William Biggs[3], Christopher D. Charles[4], Anson H. Cheung[5], Kimberly deLong[6], Isabel A. Dove[7],
548 Xiaojing Du[5,8], Emily R. Estes[9], Ursula Fuentes[10], Cristina García-Lasanta[11], Steven L.
549 Goldstein[12], Anna Golub[13], Julia Rieke Hagemann[14], Robert G. Hatfield[15], Laura L. Haynes[16],
550 Anya V. Hess[17], Nil Irvali[18], Yael Kiro[19], Minda M. Monteagudo[20], Jonathan E. Lambert[12], Chen
551 Li[21], William M. Longo[21,22], Sarah McGrath[5], Hailey Riechelson[3], Rebecca S. Robinson[7], John
552 Sarao[23], Adam D. Sproson[24], Shawn Taylor[25], Yusuke Yokoyama[26], and Siyao M. Yu[17].

553 [1]Moss Landing Marine Laboratories, Moss Landing, California, USA. [2]Center for Oceanographic
554 Research in the Eastern South Pacific (FONDAP-COPAS), University of Concepción,
555 Concepción, Chile. [3]Department of Marine and Coastal Sciences, Rutgers University, New
556 Brunswick, New Jersey, USA. [4]Scripps Institution of Oceanography, University of California, San

Diego, La Jolla, California, USA. [5]Department of Earth, Environmental, and Planetary Sciences, Brown University, Providence, Rhode Island, USA. [6]Ocean Sciences Department, University of California, Santa Cruz, Santa Cruz, California, USA. [7]University of Rhode Island Graduate School of Oceanography, Narragansett, Rhode Island, USA. [8]Institute at Brown for Environment and Society, Providence, Rhode Island, USA. [9]International Ocean Discovery Program, Texas A&M University, College Station, Texas, USA. [10]Hydrographic and Oceanographic Services, Chilean Navy, Valparaíso, Chile. [11]Geology Department, Western Washington University, Bellingham, Washington, USA. [12]Lamont-Doherty Earth Observatory, Columbia University, Palisades, New York, USA. [13]Department of Geology and Environmental Geoscience, Lafayette College, Easton, Pennsylvania, USA. [14]Department of Marine Geology and Paleontology, Alfred Wegener Institute Helmholtz Center for Polar and Marine Research, Bremerhaven, Germany. [15]Department of Geological Sciences, University of Florida, Gainesville, Florida, USA. [16]Department of Earth Science and Geography, Vassar College, Poughkeepsie, New York, USA. [17]Department of Earth and Planetary Sciences, Rutgers University, New Brunswick, New Jersey, USA. [18]Department of Earth Science and Bjerknes Centre for Climate Research, University of Bergen, Bergen, Norway. [19]Department of Earth and Planetary Sciences, Weizmann Institute of Science, Rehovot, Israel. [20]School of Earth and Atmospheric Sciences, Georgia Institute of Technology, Atlanta, Georgia, USA. [21]State Key Laboratory of Marine Geology, Tongji University, Shanghai, China. [21]Department of Environmental Studies, Macalester College, Saint Paul, Minnesota, USA. [22]Division of Environmental Health Sciences, University of Minnesota, Minneapolis, Minnesota, USA. [23]College of Geosciences, Texas A&M University, College Station, Texas, USA. [24]Biogeochemistry Research Center, JAMSTEC, Yokosuka, Japan. [25]Department of Geological Sciences and Environmental Studies, Binghamton University, Binghamton, New York, USA. [26]Atmosphere and Ocean Research Institute, The University of Tokyo, Chiba, Japan.

Data Availability Statement

The pore water, headspace, and sediment geochemical data for J1005 and J1006 can be found online at the Zenodo repository (https://doi.org/10.5281/zenodo.7160921). All correspondence and additional data requests should be addressed to V.J.C.

References

Adkins, J. F., K. McIntyre, and D. P. Schrag (2002), The salinity, temperature, and delta O-18 of the glacial deep ocean, *Science*, *298*(5599), 1769-1773, doi:10.1126/science.1076252.

Alessandrini, G., U. Tinivella, M. Giustiniani, I. de la Cruz Vargas-Cordero, and S. Castellaro (2019), Potential Instability of Gas Hydrates along the Chilean Margin Due to Ocean Warming, *Geosciences*, *9*(5), doi:10.3390/geosciences9050234.

Bangs, N. L. B., D. S. Sawyer, and X. Golovchenko (1993), Free gas at the base of the gas hydrate zone in the vicinity of the Chile Triple Junction, *Geology*, *21*(10), 905-908, doi:10.1130/0091-7613(1993)021<0905:fgatbo>2.3.co;2.

Behrmann, J., S. D. Lewis, R. J. Musgrave, and S. S. Party (1992), Proc. Ocean Drill. Prog. Initial Rep. 141, *Ocean Drilling Program, College Station TX*.

Berner, R. A. (1980), *Early diagenesis. A theoretical approach.*, 241 pp., Princeton University Press.

Bohrmann, G., J. Greinert, E. Suess, and M. E. Torres (1998), Authigenic carbonates from the Cascadia subduction zone and their relation to gas hydrate stability, *Geology*, *26*(7), 647-650.

Borowski, W. S., C. K. Paull, and W. Ussler (1996), Marine pore-water sulfate profiles indicate in situ methane flux from underlying gas hydrate, *Geology*, *24*(7), 655-658, doi:10.1130/0091-7613(1996)024<0655:mpwspi>2.3.co;2.

Boudreau, B. (1997), *Diagenetic Models and Their Implementation*, Springer-Verlag.

Bova, S. C., et al. (2019), Expedition 379T Preliminary Report, Digging Deeper with the JR100: Extending high resolution paleoclimate records from the Chilean Margin to the Eemian, *Zenodo*, doi:10.5281/zenodo.5553428.

Brown, K. M. (1990), THE NATURE AND HYDROGEOLOGIC SIGNIFICANCE OF MUD DIAPIRS AND DIATREMES FOR ACCRETIONARY SYSTEMS, *Journal of Geophysical Research-Solid Earth and Planets*, *95*(B6), 8969-8982, doi:10.1029/JB095iB06p08969.

Brown, K. M., N. L. Bangs, P. N. Froelich, and K. A. Kvenvolden (1996), The nature, distribution, and origin of gas hydrate in the Chile Triple Junction region, *Earth and Planetary Science Letters*, *139*(3-4), 471-483, doi:10.1016/0012-821x(95)00243-6.

Chan, L. H., and M. Kastner (2000), Lithium isotopic compositions of pore fluids and sediments in the Costa Rica subduction zone: Implications for fluid processes and sediment contribution to the arc volcanoes, *Earth and Planetary Science Letters*, *183*(1-2), 275-290, doi:10.1016/s0012-821x(00)00275-2.

Chao, H.-C., C.-F. You, B.-S. Wang, C.-H. Chung, and K.-F. Huang (2011), Boron isotopic composition of mud volcano fluids: Implications for fluid migration in shallow subduction zones, *Earth and Planetary Science Letters*, *305*(1-2), 32-44, doi:10.1016/j.epsl.2011.02.033.

Chen, N. C., et al. (2020), Discharge of deeply rooted fluids from submarine mud volcanism in the Taiwan accretionary prism, *Scientific Reports*, *10*(1), doi:10.1038/s41598-019-57250-9.

Clementi, V. J., et al. (2022a), Deep submarine infiltration of altered geothermal groundwater on the south Chilean Margin, *Communications Earth & Environment*, *3*(1), doi:10.1038/s43247-022-00541-3.

Clementi, V. J., Y. Rosenthal, S. C. Bova, J. D. Wright, E. K. Thomas, R. A. Mortlock, O. C. Cowling, L. V. Godfrey, L. B. Childress, and E. T. Scientists (2022b), Pore water and headspace gas data for Sites J1005 and J1006 on the south Chilean Margin, edited, Zenodo, doi:10.5281/zenodo.7160921.

Coffin, R., J. Pohlman, J. Gardner, R. Downer, W. Wood, L. Hamdan, S. Walker, R. Plummer, J. Gettrust, and J. Diaz (2007), Methane hydrate exploration on the mid Chilean coast: A

geochemical and geophysical survey, *Journal of Petroleum Science and Engineering*, *56*(1-3), 32-41, doi:10.1016/j.petrol.2006.01.013.

Contreras-Reyes, E., J. Jara, A. Maksymowicz, and W. Weinrebe (2013), Sediment loading at the southern Chilean trench and its tectonic implications, *Journal of Geodynamics*, *66*, 134-145, doi:10.1016/j.jog.2013.02.009.

Dahlmann, A., and G. J. de Lange (2003), Fluid-sediment interactions at Eastern Mediterranean mud volcanoes: a stable isotope study from ODP Leg 160, *Earth and Planetary Science Letters*, *212*(3-4), 377-391, doi:10.1016/s0012-821x(03)00227-9.

Davidson, D. W., D. G. Leaist, and R. Hesse (1983), Oxygen-18 enrichment in the water of a clathrate hydrate, *Geochimica et Cosmochimica Acta*, *47*(12), 2293-2295, doi:10.1016/0016-7037(83)90053-4.

Deyhle, A., and A. Kopf (2001), Deep fluids and ancient pore waters at the backstop: Stable isotope systematics (B, C, O) of mud-volcano deposits on the Mediterranean Ridge accretionary wedge, *Geology*, *29*(11), 1031-1034, doi:10.1130/0091-7613(2001)029<1031:dfaapw>2.0.co;2.

Dia, A. N., M. Castrec-Rouelle, J. Boulegue, and P. Comeau (1999), Trinidad mud volcanoes: Where do the expelled fluids come from?, *Geochimica Et Cosmochimica Acta*, *63*(7-8), 1023-1038, doi:10.1016/s0016-7037(98)00309-3.

Egeberg, P. K., P. Aagaard, and P. C. Smalley (1990), Major element and oxygen isotope studies of interstitial waters: ODP Leg 113, *Proceedings of the Ocean Drilling Program, Scientific Results*, *113*.

Egeberg, P. K., and G. R. Dickens (1999), Thermodynamic and pore water halogen constraints on gas hydrate distribution at ODP Site 997 (Blake Ridge), *Chemical Geology*, *153*(1-4), 53-79, doi:10.1016/s0009-2541(98)00152-1.

Elderfield, H., and J. M. Gieskes (1982), Sr isotopes in interstitial waters of marine sediments from Deep Sea Drilling Project cores, *Nature*, *300*(5892), 493-497, doi:10.1038/300493a0.

Elderfield, H., M. Kastner, and J. B. Martin (1990), Compositions and sources of fluids in sediments of the Peru Subduction Zone, *Journal of Geophysical Research*, *95*(B6), 8819, doi:10.1029/jb095ib06p08819.

Epstein, S., and T. Mayeda (1953), Variation of O18 content of waters from natural sources, *Geochimica et Cosmochimica Acta*, *4*(5), 213-224, doi:10.1016/0016-7037(53)90051-9.

Fairbanks, R. G. (1982), The origin of continental shelf and slope water in the New York Bight and Gulf of Mexico: evidence from $H_2^{18}O/H_2^{16}O$ ratio measurements, *Journal of Geophysical Research*, *87*, 5796-5808.

Fournier, R. O. (1979), A revised equation for the Na/K geothermometer, *Geothermal Reserouces Council Transactions*, *3*, 221-224.

Garreaud, R., P. Lopez, M. Minvielle, and M. Rojas (2013), Large-Scale Control on the Patagonian Climate, *Journal of Climate*, *26*(1), 215-230, doi:10.1175/jcli-d-12-00001.1.

Geersen, J., J. H. Behrmann, D. Völker, S. Krastel, C. R. Ranero, J. Diaz-Naveas, and W. Weinrebe (2011), Active tectonics of the South Chilean marine fore arc (35°S-40°S), *Tectonics*, *30*(3), n/a-n/a, doi:10.1029/2010tc002777.

Geersen, J., F. Scholz, P. Linke, M. Schmidt, D. Lange, J. H. Behrmann, D. Volker, and C. Hensen (2016), Fault zone controlled seafloor methane seepage in the rupture area of the 2010 Maule earthquake, Central Chile, *Geochemistry Geophysics Geosystems*, *17*(11), 4802-4813, doi:10.1002/2016gc006498.

Gieskes, J., et al. (1989), HYDROGEOCHEMISTRY IN THE BARBADOS ACCRETIONARY COMPLEX - LEG-110 ODP, *Palaeogeography Palaeoclimatology Palaeoecology*, *71*(1-2), 83-96, doi:10.1016/0031-0182(89)90031-x.

Gieskes, J., T. Gamo, and H. J. Brumsack (1991), Chemical methods for interstitial water analysis aboard JOIDES Resolution, *ODP Technical Note*, *15*.

Godon, A., N. Jendrzejewski, M. Castrec-Rouelle, A. Dia, F. Pineau, J. Boulegue, and M. Javoy (2004), Origin and evolution of fluids from mud volcanoes in the Barbados accretionary complex, *Geochimica Et Cosmochimica Acta*, *68*(9), 2153-2165, doi:10.1016/j.gca.2003.08.021.

Haese, R. R., C. Hensen, and G. J. de Lange (2006), Pore water geochemistry of eastern Mediterranean mud volcanoes: Implications for fluid transport and fluid origin, *Marine Geology*, *225*(1-4), 191-208, doi:10.1016/j.margeo.2005.09.001.

Hensen, C., M. Nuzzo, E. Hornibrook, L. M. Pinheiro, B. Bock, V. H. Magalhaes, and W. Bruckmann (2007), Sources of mud volcano fluids in the Gulf of Cadiz - indications for hydrothermal imprint, *Geochimica Et Cosmochimica Acta*, *71*(5), 1232-1248, doi:10.1016/j.gca.2006.11.022.

Hesse, R., and W. Harrison (1981), Gas hydrates (clathrates) causing pore-water freshening and oxygen isotope fractionation in deep-water sedimentary sections of terrigenous continental margins, *Earth and Planetary Science Letters*, *55*, 453-462.

Holmes, A. M., P. G. Oliver, and J. Sellanes (2005), A new species of Lucinoma (Bivalvia : Lucinoidea) from a methane gas seep off the southwest coast of Chile, *Journal of Conchology*, *38*, 673-681.

Hong, W. L., T. Pape, C. Schmidt, H. Yao, K. Wallmann, A. Plaza-Faverola, J. W. B. Rae, A. Lepland, S. Bunz, and G. Bohrmann (2021), Interactions between deep formation fluid and gas hydrate dynamics inferred from pore fluid geochemistry at active pockmarks of the Vestnesa Ridge, west Svalbard margin, *Marine and Petroleum Geology*, *127*, doi:10.1016/j.marpetgeo.2021.104957.

Hong, W. L., M. E. Torres, and S. Kutterolf (2020), Towards a global quantification of volcanogenic aluminosilicate alteration rates through the mass balance of strontium in marine sediments, *Chemical Geology*, *550*, 119743, doi:10.1016/j.chemgeo.2020.119743.

Horwitz, E. P., R. Chiarizia, and M. L. Dietz (1992), A NOVEL STRONTIUM-SELECTIVE EXTRACTION CHROMATOGRAPHIC RESIN, *Solvent Extraction and Ion Exchange*, *10*(2), 313-336, doi:10.1080/07366299208918107.

Hüpers, A., and A. J. Kopf (2012), Effect of smectite dehydration on pore water geochemistry in the shallow subduction zone: An experimental approach, *Geochemistry, Geophysics, Geosystems*, *13*(10), n/a-n/a, doi:10.1029/2012gc004212.

Kastner, M., H. Elderfield, and J. B. Martin (1991), FLUIDS IN CONVERGENT MARGINS - WHAT DO WE KNOW ABOUT THEIR COMPOSITION, ORIGIN, ROLE IN DIAGENESIS AND IMPORTANCE FOR OCEANIC CHEMICAL FLUXES, *Philosophical Transactions of the Royal Society of London Series a-Mathematical Physical and Engineering Sciences*, *335*(1638), 243-259, doi:10.1098/rsta.1991.0045.

Kastner, M., H. Elderfield, J. B. Martin, E. Suess, K. A. Kvenvolden, and R. E. Garrison (1990), Diagenesis and interstitial water chemistry at the Peruvian continental margin: Major constituents and strontium isotopes, *Proceedings of the Ocean Drilling Program*, *112*, 413-440.

Klaucke, I., W. Weinrebe, P. Linke, D. Klaschen, and J. Bialas (2012), Sidescan sonar imagery of widespread fossil and active cold seeps along the central Chilean continental margin, *Geo-Marine Letters*, *32*(5-6), 489-499, doi:10.1007/s00367-012-0283-1.

Kopf, A. J. (2002), SIGNIFICANCE OF MUD VOLCANISM, *Reviews of Geophysics*, *40*(2), 2-1-2-52, doi:10.1029/2000rg000093.

Kopf, A. J., and A. Deyhle (2002), Back to the roots: boron geochemistry of mud volcanoes and its implications for mobilization depth and global B cycling, *Chemical Geology*, *192*(3-4), 195-210, doi:10.1016/s0009-2541(02)00221-8.

Kvenvolden, K. A. (1993), Gas Hydrates—Geological Perspective and Global Change, *Rev. Geophys.*, *31*(2), 173-187.

Kvenvolden, K. A., and M. Kastner (1990), Gas hydrates of the Peruvian outer continental margin, *Proceedings of the Ocean Drilling Program, Scientific Results*, *112*, 517-526.

Lamy, F., D. Hebbeln, and G. Wefer (1998), Terrigenous sediment supply along the Chilean continental margin: modern regional patterns of texture and composition, *Geol Rundsch*, *87*, 477-494.

Lawrence, J. R., and J. M. Gieskes (1981), Constraints on water transport and alteration in the oceanic crust from the isotopic composition of pore water, *Journal of Geophysical Research: Solid Earth*, *86*(B9), 7924-7934, doi:10.1029/jb086ib09p07924.

Li, Y. H., and S. Gregory (1974), Diffusion of ions in sea water and in deep-sea sediments, *Geochimica et Cosmochimica Acta*, *38*(5), 703-714, doi:10.1016/0016-7037(74)90145-8.

Maksymowicz, A. (2015), The geometry of the Chilean continental wedge: Tectonic segmentation of subduction processes off Chile, *Tectonophysics*, *659*, 183-196, doi:10.1016/j.tecto.2015.08.007.

Martin, J. B., M. Kastner, P. Henry, X. Le Pichon, and S. Lallement (1996), Chemical and isotopic evidence for sources of fluids in a mud volcano field seaward of the Barbados accretionary wedge, *Journal of Geophysical Research: Solid Earth*, *101*(B9), 20325-20345, doi:10.1029/96jb00140.

Matsumoto, R., and W. S. Borowski (2000), GAS HYDRATE ESTIMATES FROM NEWLY DETERMINED OXYGEN ISOTOPIC FRACTIONATION (α_{GH-IW}) AND $\delta^{18}O$ ANOMALIES OF THE INTERSTITIAL WATERS: LEG 164, BLAKE RIDGE, *Proceedings of the Ocean Drilling Program, Scientific Results*, *164*, 59-66.

Melnick, D., B. Bookhagen, H. P. Echtler, and M. R. Strecker (2006), Coastal deformation and great subduction earthquakes, Isla Santa Maria, Chile (37 degrees S), *Geological Society of America Bulletin*, *118*(11-12), 1463-1480, doi:10.1130/b25865.1.

Menapace, W., D. Volker, N. Kaul, M. D. Tryon, and A. J. Kopf (2017), The role of mud volcanism and deep-seated dewatering processes in the Nankai Trough accretionary prism and Kumano Basin, Japan, *Geochemistry Geophysics Geosystems*, *18*(7), 2486-2509, doi:10.1002/2016gc006763.

Milkov, A. V. (2000), Worldwide distribution of submarine mud volcanoes and associated gas hydrates, *Marine Geology*, *167*(1-2), 29-42, doi:10.1016/s0025-3227(00)00022-0.

Mix, A. C., R. Tiedemann, P. Blum, and a. C. Participants (2003), Initial Reports, *Proceedings of the Ocean Drilling Program*, *202*, doi:doi:10.2973/odp.proc.ir.202.2003.

Moore, J. C., and P. Vrolijk (1992), FLUIDS IN ACCRETIONARY PRISMS, *Reviews of Geophysics*, *30*(2), 113-135, doi:10.1029/92rg00201.

Munoz, P., L. J. Cardenas, D. Garbe-Schonberg, J. Sellanes, L. Dezileau, I. Melville, and S. D. Mendes (2016), Geochemical characterization of two distinctive systems with evidence of

chemosynthetic activity, explored at the SE Pacific margin off Chile (46 degrees S and 33 degrees S), *Progress in Oceanography*, *148*, 26-43, doi:10.1016/j.pocean.2016.09.002.

Murray, R. W., D. J. Miller, and K. A. Kryc (2000), Analysis of major and trace elements in rocks, sediments, and interstitial waters by inductively coupled plasma-atomic emission spectrometry (ICP-AES), *ODP Technical Note*, *29*.

Nieva, D., and R. Nieva (1987), Developments in geothermal energy in Mexico—part twelve. A cationic geothermometer for prospecting of geothermal resources, *Heat Recovery Systems and CHP*, *7*(3), 243-258, doi:10.1016/0890-4332(87)90138-4.

Nishio, Y., A. Ijiri, T. Toki, Y. Morono, M. Tanimizu, K. Nagaishi, and F. Inagaki (2015), Origins of lithium in submarine mud volcano fluid in the Nankai accretionary wedge, *Earth and Planetary Science Letters*, *414*, 144-155, doi:10.1016/j.epsl.2015.01.018.

Peacock, S. M. (1990), FLUID PROCESSES IN SUBDUCTION ZONES, *Science*, *248*(4953), 329-337, doi:10.1126/science.248.4953.329.

Perry, E. (1970), Burial Diagenesis in Gulf Coast Pelitic Sediments, *Clays and Clay Minerals*, *18*(3), 165-177, doi:10.1346/ccmn.1970.0180306.

Reeburgh, W. S. (1980), Anaerobic methane oxidation: Rate depth distributions in Skan Bay sediments, *Earth and Planetary Science Letters*, *47*(3), 345-352, doi:10.1016/0012-821x(80)90021-7.

Rodrigo, C., A. Gonzalez-Fernandez, and E. Vera (2009), Variability of the bottom-simulating reflector (BSR) and its association with tectonic structures in the Chilean margin between Arauco Gulf (37 degrees S) and Valdivia (40 degrees S), *Marine Geophysical Researches*, *30*(1), 1-19, doi:10.1007/s11001-009-9064-2.

Saffer, D. M., and H. J. Tobin (2011), Hydrogeology and Mechanics of Subduction Zone Forearcs: Fluid Flow and Pore Pressure, in *Annual Review of Earth and Planetary Sciences, Vol 39*, edited by R. Jeanloz and K. H. Freeman, pp. 157-186, Annual Reviews, Palo Alto, doi:10.1146/annurev-earth-040610-133408.

Sample, J. C. (1996), Isotopic evidence from authigenic carbonates for rapid upward fluid flow in accretionary wedges, *Geology*, *24*(10), 897-900, doi:10.1130/0091-7613(1996)024<0897:iefacf>2.3.co;2.

Scholz, F., C. Hensen, A. Reitz, R. L. Romer, V. Liebetrau, A. Meixner, S. M. Weise, and M. Haeckel (2009), Isotopic evidence (87Sr/86Sr, δ7Li) for alteration of the oceanic crust at deep-rooted mud volcanoes in the Gulf of Cadiz, NE Atlantic Ocean, *Geochimica et Cosmochimica Acta*, *73*(18), 5444-5459, doi:10.1016/j.gca.2009.06.004.

Scholz, F., C. Hensen, M. Schmidt, and J. Geersen (2013), Submarine weathering of silicate minerals and the extent of pore water freshening at active continental margins, *Geochimica et Cosmochimica Acta*, *100*, 200-216, doi:10.1016/j.gca.2012.09.043.

Sellanes, J., E. Quiroga, and V. A. Gallardo (2004), First direct evidence of methane seepage and associated chemosynthetic communities in the bathyal zone off Chile, *Journal of the Marine Biological Association of the United Kingdom*, *84*(5), 1065-1066, doi:10.1017/s0025315404010422h.

Sellanes, J., E. Quiroga, and C. Neira (2008), Megafauna community structure and trophic relationships at the recently discovered Concepción Methane Seep Area, Chile, ~36°S, *ICES Journal of Marine Science*, *65*(7), 1102-1111, doi:10.1093/icesjms/fsn099.

Toki, T., M. Kinoshita, S. Morita, H. Masuda, H. Rashid, H. Yoshinishi, T. Nakano, and T. Noguchi (2017), The vertical chloride ion profile at the IODP Site C0002, Kumano Basin, off coast of Japan, *Tectonophysics*, *710*, 88-96, doi:10.1016/j.tecto.2016.11.029.

Tomaru, H., M. E. Torres, R. Matsumoto, and W. S. Borowski (2006), Effect of massive gas hydrate formation on the water isotopic fractionation of the gas hydrate system at Hydrate Ridge, Cascadia margin, offshore Oregon, *Geochemistry, Geophysics, Geosystems*, *7*(10), n/a-n/a, doi:10.1029/2005gc001207.

Tonani, F. B. (1980), Some Remarks on the Application of Geochemical Techniques in geothermal exploration, in *Advances in European Geothermal Research*, edited, pp. 428-443, Springer Netherlands, doi:10.1007/978-94-009-9059-3_38.

Torres, M. E., W. L. Hong, E. A. Solomon, K. Milliken, J. H. Kim, J. C. Sample, B. M. A. Teichert, and K. Wallmann (2020), Silicate weathering in anoxic marine sediment as a requirement for authigenic carbonate burial, *Earth-Science Reviews*, *200*, 15, doi:10.1016/j.earscirev.2019.102960.

Torres, M. E., B. M. A. Teichert, A. M. Trehu, W. Borowski, and H. Tomaru (2004), Relationship of pore water freshening to accretionary processes in the Cascadia margin: Fluid sources and gas hydrate abundance, *Geophysical Research Letters*, *31*(22), 4, doi:10.1029/2004gl021219.

Treude, T., J. Niggemann, J. Kallmeyer, P. Wintersteller, C. J. Schubert, A. Boetius, and B. B. Jørgensen (2005), Anaerobic oxidation of methane and sulfate reduction along the Chilean continental margin, *Geochimica et Cosmochimica Acta*, *69*(11), 2767-2779, doi:10.1016/j.gca.2005.01.002.

Ussler, W., and C. K. Paull (1995), EFFECTS OF ION-EXCLUSION AND ISOTOPIC FRACTIONATION ON PORE-WATER GEOCHEMISTRY DURING GAS HYDRATE FORMATION AND DECOMPOSITION, *Geo-Marine Letters*, *15*(1), 37-44, doi:10.1007/bf01204496.

van Geldern, R., and J. A. C. Barth (2012), Optimization of instrument setup and post-run corrections for oxygen and hydrogen stable isotope measurements of water by isotope ratio infrared spectroscopy (IRIS), *Limnology and Oceanography-Methods*, *10*, 1024-1036, doi:10.4319/lom.2012.10.1024.

Vanneste, H., B. A. Kelly-Gerreyn, D. P. Connelly, R. H. James, M. Haeckel, R. E. Fisher, K. Heeschen, and R. A. Mills (2011), Spatial variation in fluid flow and geochemical fluxes across the sediment-seawater interface at the Carlos Ribeiro mud volcano (Gulf of Cadiz), *Geochimica Et Cosmochimica Acta*, *75*(4), 1124-1144, doi:10.1016/j.gca.2010.11.017.

Vargas-Cordero, I., U. Tinivella, F. Accaino, M. F. Loreto, and F. Fanucci (2010), Thermal state and concentration of gas hydrate and free gas of Coyhaique, Chilean Margin (44°30′ S), *Marine and Petroleum Geology*, *27*(5), 1148-1156, doi:10.1016/j.marpetgeo.2010.02.011.

Vargas-Cordero, I., U. Tinivella, L. Villar-Munoz, J. P. Bento, C. Carcamo, D. Lopez-Acevedo, F. Fernandoy, A. Rivero, and M. S. Juan (2020), Gas hydrate versus seabed morphology offshore Lebu (Chilean margin), *Scientific Reports*, *10*(1), doi:10.1038/s41598-020-78958-z.

Vargas-Cordero, I., U. Tinivella, and L. Villar-Muñoz (2017), Gas Hydrate and Free Gas Concentrations in Two Sites inside the Chilean Margin (Itata and Valdivia Offshores), *Energies*, *10*(12), doi:10.3390/en10122154.

Vargas-Cordero, I., U. Tinivella, L. Villar-Muñoz, and J. Bento (2018), High Gas Hydrate and Free Gas Concentrations: An Explanation for Seeps Offshore South Mocha Island, *Energies*, *11*(11), 3062, doi:10.3390/en11113062.

Vargas-Cordero, I., L. Villar-Muñoz, U. Tinivella, M. Giustiniani, N. Bangs, J. P. Bento, and E. Contreras-Reyes (2021), Gas origin linked to paleo BSR, *Scientific Reports*, *11*(1), doi:10.1038/s41598-021-03371-z.

Villar-Muñoz, L., J. P. Bento, D. Klaeschen, U. Tinivella, I. d. l. C. Vargas-Cordero, and J. H. Behrmann (2018), A first estimation of gas hydrates offshore Patagonia (Chile), *Marine and Petroleum Geology*, *96*, 232-239, doi:10.1016/j.marpetgeo.2018.06.002.

Villar-Muñoz, L., et al. (2021), A cold seep triggered by a hot ridge subduction, *Scientific Reports*, *11*(1), doi:10.1038/s41598-021-00414-3.

Villar-Muñoz, L., I. Vargas-Cordero, J. Bento, U. Tinivella, F. Fernandoy, M. Giustiniani, J. Behrmann, and S. Calderón-Díaz (2019), Gas Hydrate Estimate in an Area of Deformation and High Heat Flow at the Chile Triple Junction, *Geosciences*, *9*(1), doi:10.3390/geosciences9010028.

Völker, D., H. Wehrmann, S. Kutterolf, K. Iyer, W. Rabbel, J. Geersen, and K. Hoernle (2014), Constraining input and output fluxes of the southern-central Chile subduction zone: water, chlorine and sulfur, *International Journal of Earth Sciences*, *103*(7), 2129-2153, doi:10.1007/s00531-014-1002-0.

Völker, D., J. Geersen, E. Contreras-Reyes, and C. Reichert (2013), Sedimentary fill of the Chile Trench (32–46°S): volumetric distribution and causal factors, *Journal of the Geological Society*, *170*(5), 723-736, doi:10.1144/jgs2012-119.

Völker, D., J. Geersen, E. Contreras-Reyes, J. Sellanes, S. Pantoja, W. Rabbel, M. Thorwart, C. Reichert, M. Block, and W. R. Weinrebe (2014), Morphology and geology of the continental shelf and upper slope of southern Central Chile (33°S–43°S), *International Journal of Earth Sciences*, *103*(7), 1765-1787, doi:10.1007/s00531-012-0795-y.

Völker, D., I. Grevemeyer, M. Stipp, K. Wang, and J. He (2011), Thermal control of the seismogenic zone of southern central Chile, *Journal of Geophysical Research*, *116*(B10), doi:10.1029/2011jb008247.

Völker, D., and M. Stipp (2015), Water input and water release from the subducting Nazca Plate along southern Central Chile (33°S-46°S), *Geochemistry, Geophysics, Geosystems*, *16*(6), 1825-1847, doi:10.1002/2015gc005766.

Wallmann, K., G. Aloisi, M. Haeckel, P. Tishchenko, G. Pavlova, J. Greinert, S. Kutterolf, and A. Eisenhauer (2008), Silicate weathering in anoxic marine sediments, *Geochimica Et Cosmochimica Acta*, *72*(12), 2895-2918, doi:10.1016/j.gca.2008.03.026.

Waseda, A. (1998), Organic carbon content, bacterial methanogenesis, and accumulation processes of gas hydrates in marine sediments., *GEOCHEMICAL JOURNAL*, *32*(3), 143-157, doi:10.2343/geochemj.32.143.

You, K., P. B. Flemings, A. Malinverno, T. S. Collett, and K. Darnell (2019), Mechanisms of Methane Hydrate Formation in Geological Systems, *Reviews of Geophysics*, doi:10.1029/2018rg000638.

Zheng, Y., P. N. Froelich, M. E. Torres, and A. N. Dia (1995), Stable Isotopes (18-O/16-O) and 87-Sr/86-Sr Ratios in Pore Fluids of the Chile Triple Junction Accretionary Prism: Implications for Diagenesis and Fluid Migration, in *Proceedings of the Ocean Drilling Program, Scientific Results*, edited by S. D. Lewis, J. H. Behrmann, R. J. Musgrave and S. C. Cande.

Figure 1: Study Setting. A) Bathymetric map of regional study area with the location of Sites J1005 (blue), J1006 (dark grey), and ODP Site 1233 (yellow) denoted by the colored symbols. Dotted line represents the seismic profile in C and D. Red symbol represents the general location of a gas flare shown in panel D. B) Downcore pore water chloride (Cl$^-$) concentration at the three sites, with the same color assignment in A. Depth scale in meters below sea floor (mbsf). Black arrow marks seawater concentration. C) Underway seismic profile of the study area along the A-A' line shown in subpanel A. Site J1006 is located on a ~4 km wide, 25 m tall seafloor mound, with ODP Site 1233 slightly to the north and Site J1005 positioned just upslope to the south. D) Underway seismic profile of the study area along the B-B' line shown in subpanel A, with ODP Site 1233, the observed gas flare, and seismic blanking feature shown. For C and D, images have been modified with permission after Hebbeln et al. [1995].

Figure 2: Pore water geochemistry at Site J1005. Downcore profiles for SO$_4^{2-}$, headspace CH$_4$ concentrations, alkalinity, NH$_4^+$, Cl$^-$, Na/Cl, Ca/Cl, Mg/Cl, K/Cl, B/Cl, DSi/Cl, Li/Cl, Sr/Cl, δ^{18}O, δD, and ^{87}Sr/^{86}Sr. For δ^{18}O, squares are samples measured via Picarro and open circles are samples measured via mass spectrometer. Reported errors for δ^{18}O, δD, and ^{87}Sr/^{86}Sr represent 1 SD; uncertainty is smaller than the symbol size.

Figure 3: Pore water geochemistry at Site J1006. Downcore profiles for SO$_4^{2-}$, headspace CH$_4$ concentrations, alkalinity, NH$_4^+$, Cl$^-$, Na/Cl, Ca/Cl, Mg/Cl, K/Cl, B/Cl, DSi/Cl, Li/Cl, Sr/Cl, δ^{18}O, δD, and ^{87}Sr/^{86}Sr. For δ^{18}O, squares are samples measured via Picarro and open circles are samples measured via mass spectrometer. Reported errors for δ^{18}O, δD, and ^{87}Sr/^{86}Sr represent 1 SD; uncertainty is smaller than the symbol size.

Figure 4: Changes in pore water δ^{18}O and δD as a function of freshening. Differences in δ^{18}O (A) and δD (B) between downcore observations (δ_{obs}) and seawater reference (δ_{ref}) values ($\Delta\delta^{18}$O and $\Delta\delta$D, respectively) plotted against pore water Cl$^-$ normalized to seawater (f([Cl$_{obs}$]/[Cl$_{ref}$]). Site J1005 (blue) and J1006 (dark grey) are shown. Seawater reference values are denoted by the red star.

Figure 5: Strontium systematics at Sites J1005 and J1006. Pore water ^{87}Sr/^{86}Sr plotted against the inverse Sr concentration for Site J1005 (blue) and J1006 (dark grey). The seawater reference value is denoted by the red star. The schematic inset indicates the general direction of change associated with marine silicate weathering (MSiW), authigenic carbonate precipitation, and ash diagenesis.

Figure 6: Spatially variable pore water geochemistry near the mound. Downcore profiles for concentrations of SO$_4^{2-}$ (A), headspace methane (B), alkalinity (C), Cl$^-$ (D), K (E), and Li (F) at Sites J1005 (blue), J1006 (dark grey), and ODP Site 1233 (yellow). In A, the inset figure shows

SO_4^{2-} concentrations between the seafloor and 15 mbsf. Solid lines denote linear gradients used in sulfate diffusion calculations.

Figure 7: A conceptual schematic for fluid migration and methane hydrate formation near the regional venting structure. The location of J1005, J1006, and ODP 1233 are shown in proximity to the mound feature. The red line marks the assumed shape of the mound feature based on sediment and pore water data. Large blue arrows denote the vertical migration of deep-sourced fluids from clay dehydration at depth with its characteristic low-Cl^-, high $\delta^{18}O$, and low δD signatures. The white symbols with "GH" represent approximate depths that methane hydrate was recovered at Site J1006, for which their occurrence might be linked to high methane fluxes close to the mound (see inset CH_4 flux plot). Dotted blue lines denote additional likely pathways for fluid being expelled at the venting structure based on low-Cl^- below 60 mbsf at ODP Site 1233 and high $\delta^{18}O$/lowδD in the deepest data point at J1005. However, the lack of concomitant freshening in this sample leaves this pathway relatively unconstrained. This figure has been modified with permission after Hebbeln et al. [1995].
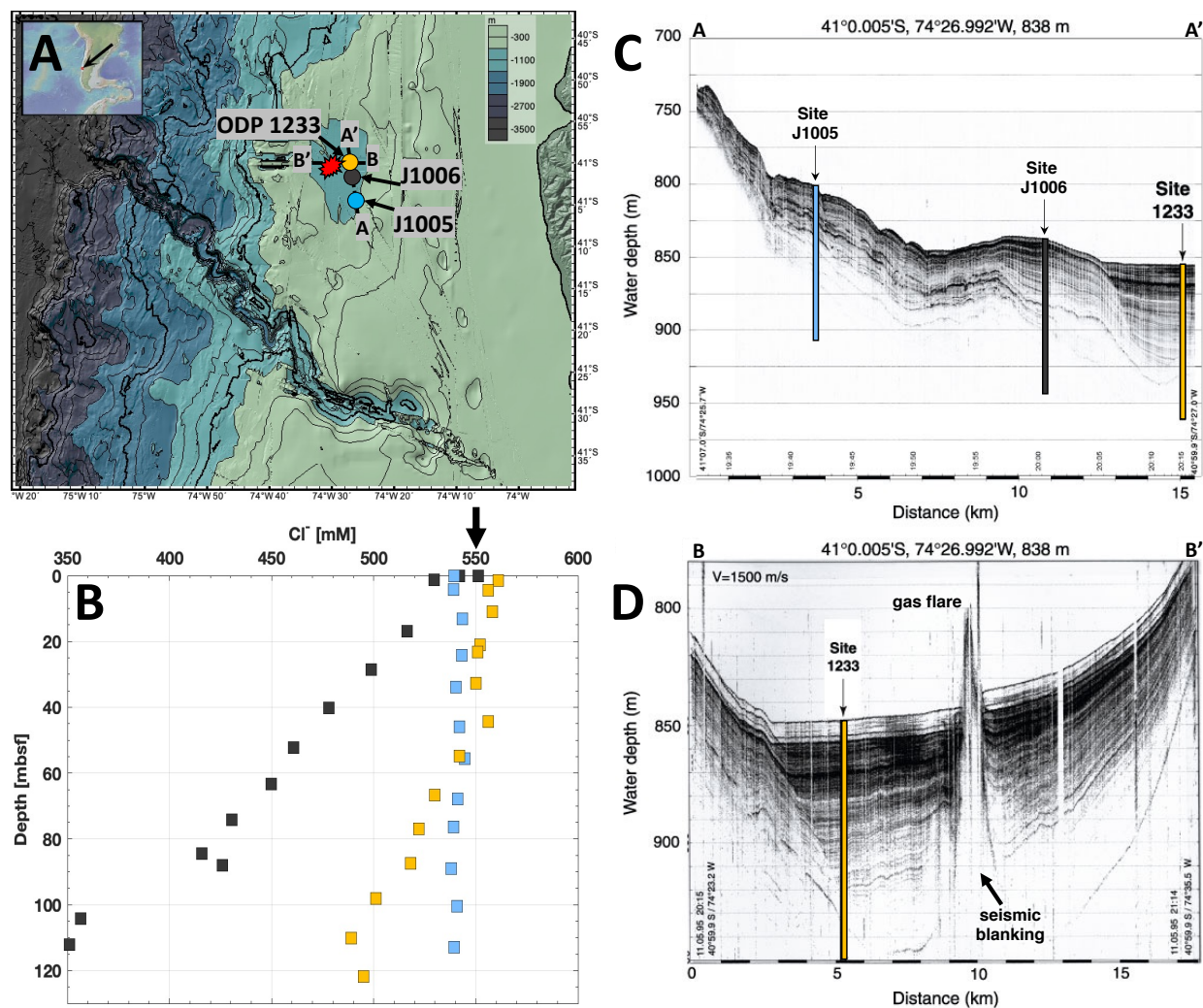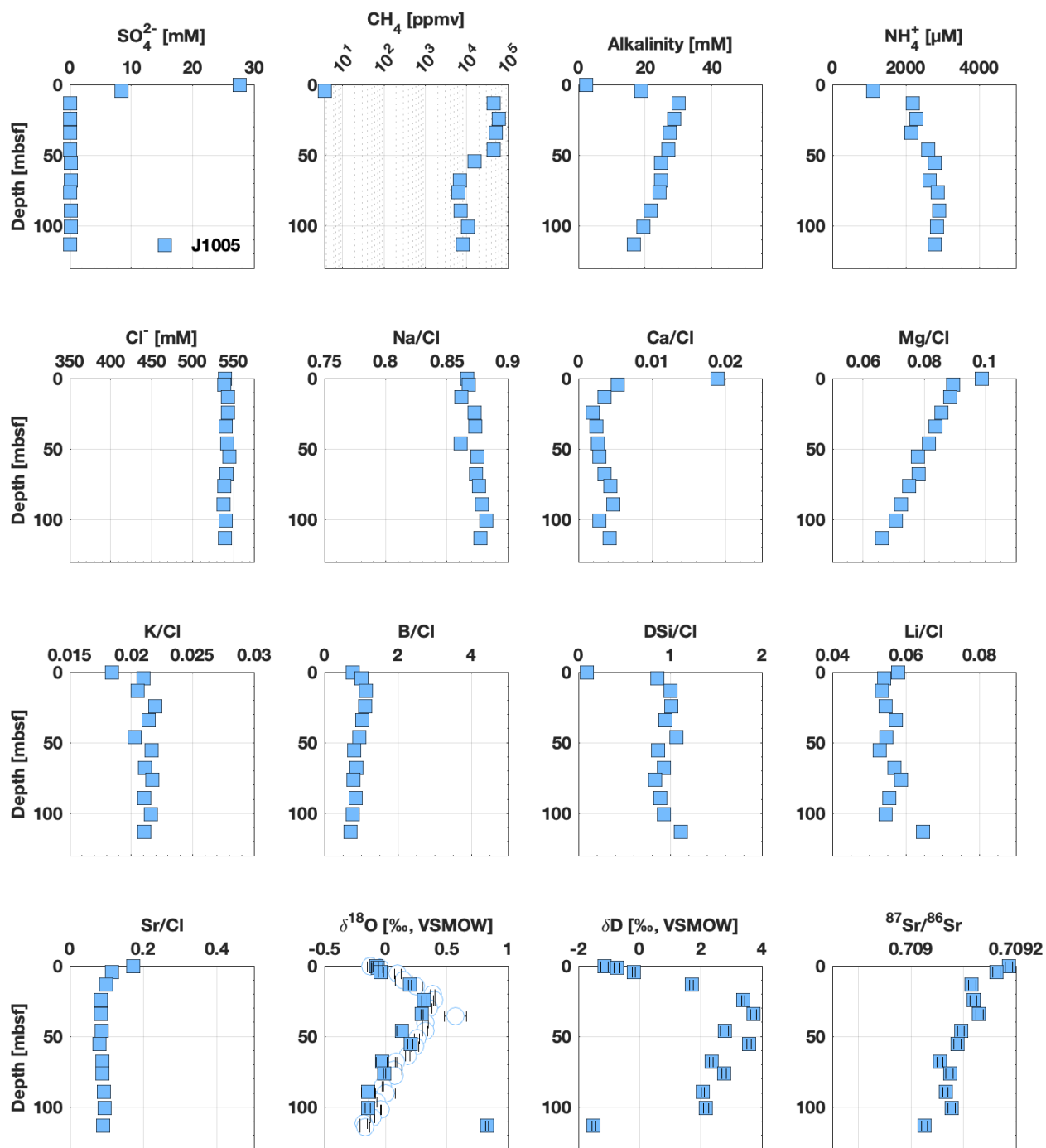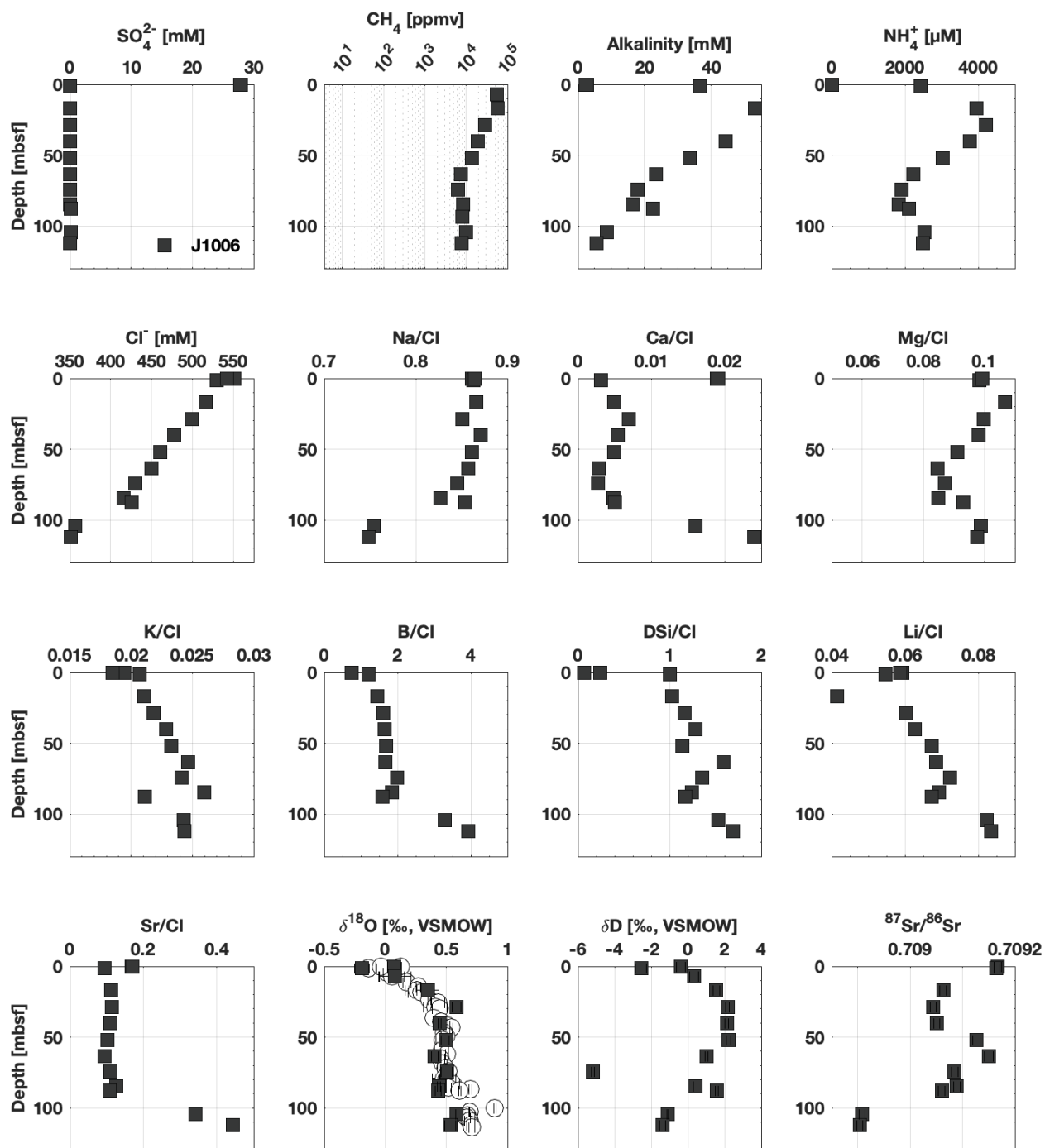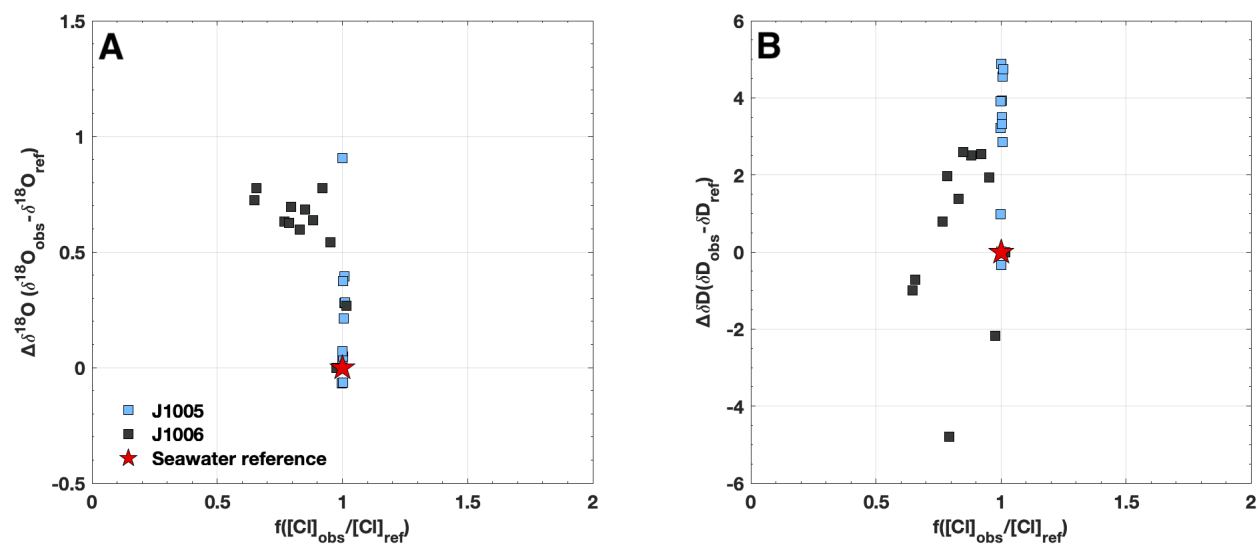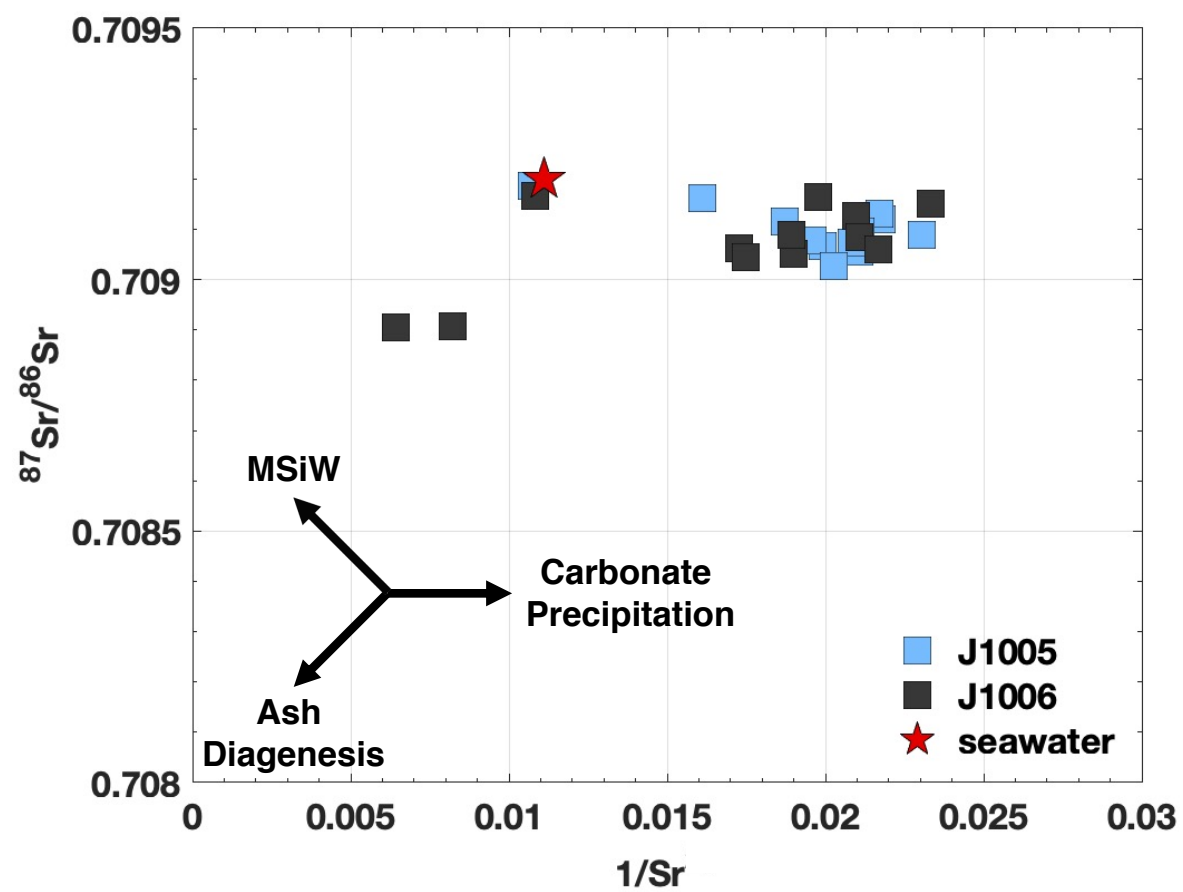
Figure 1

Figure 2

Figure 3

Figure 4

Figure 5
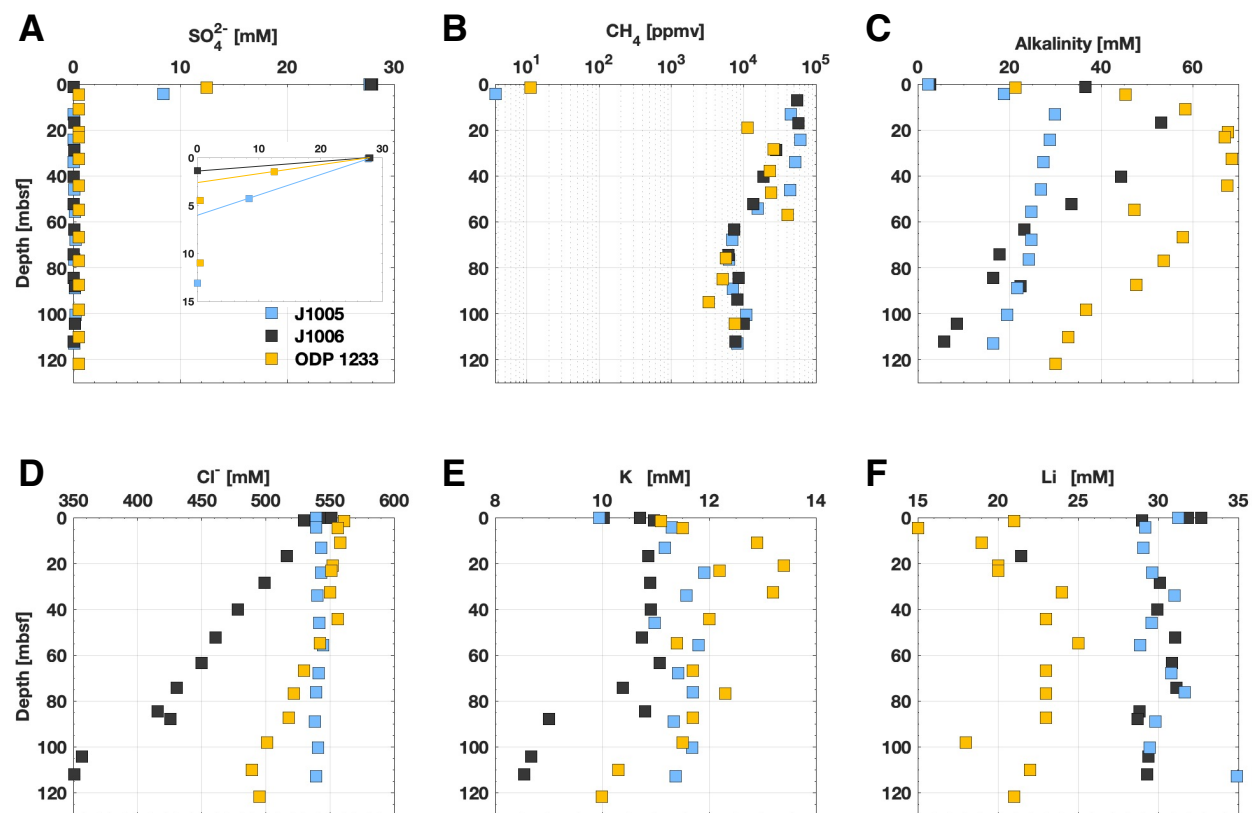
Figure 6
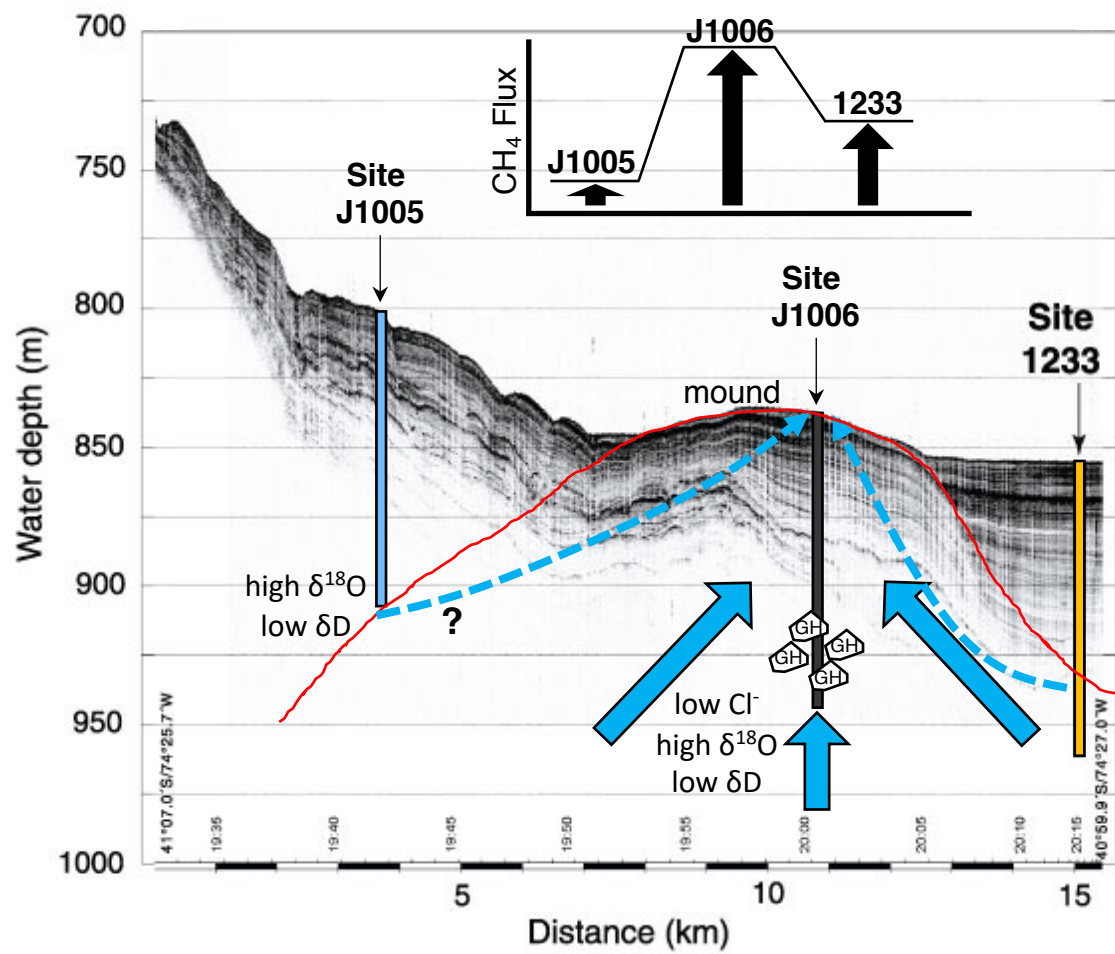
Figure 7

Table 1: Core locations, water depth, and proximity to the mound venting structure at 41°S						
Site	Latitude	Longitude	Water Depth (m)	Distance to Mound (km)	Estimated Bottom Age (kyr)	Reference
J1005	41°4.58'S	74°26.70'W	807	5-10	170	This Study
J1006	41°1.56'S	74°26.70'W	824	~0	70	This Study
ODP 1233	41°0.00'S	74°26.99'W	838	<5	70	Mix et al. [2003]

Table 2: Estimates for the depth of illitization at 41°S based on Na/K geothermometry							
Site	Geothermal Gradient (°C km^{-1})	Na/K (°C)[c]	$Z_{S \to I}$ (kmbsf)[c]	Na/K (°C)[d]	$Z_{S \to I}$ (kmbsf)[d]	Na/K (°C)[e]	$Z_{S \to I}$ (kmbsf)[e]
J1005[a]	57	138±3	2.4	133±4	2.3	150±3	2.6
J1006[a]	76	146±9	1.9	143±11	1.9	158±9	2.1
ODP 1233[b]	45	142±4	3.2	138±5	3.1	154±4	3.4
[a][*Bova et al.*, 2019] [b][*Grevemeyer et al.*, 2003] [c][*Nieva and Nieva*, 1987] [d][*Tonani*, 1980] [e][*Fournier*, 1979] *Note: All concentrations in mg/L. Reported errors represent 1 SD.*							

Table 3: SMTZ depth, changes in pore water sulfate concentration, diffusive sulfate fluxes, near the mound			
Site	SMTZ (mbsf)	$\Delta[SO_4^{2-}]$ (mM)	Flux (mM SO_4^{2-} m^{-2} yr^{-1})
J1005	6	27.712	-67.40
J1006	1.35	27.965	-306.96
ODP 1233	2.5	27.5	-164.63